Topological edge states of continuous Hamiltonians

Matthew Frazier [*]   Guillaume Bal [†]

March 18, 2025

Abstract

This paper concerns the topological classification of continuous Hamiltonians that find applications in biased cold plasmas and photonics. Besides a magnetic bias, the Hamiltonians are parametrized by a plasma frequency and a fixed vertical wavenumber. Eight distinct phases of matter are identified as these parameters vary. When insulating gaps are shared by two such phases, asymmetric edge modes propagate along interfaces separating the phases. Here we apply the notion of a bulk difference invariant (BDI) to this Hamiltonian, and show by numerical diagonalizations of interface Hamiltonians that after an appropriate regularization our BDI correctly predicts edge transport as described by a bulk edge correspondence. We also derive theoretical tools to compute the BDI and show the limitations of the bulk edge correspondence (BEC) when the phase transition is too singular.

1   Introduction

Topological systems display phases of transport characterized by topological invariants and, as a consequence, are robust to large classes of perturbations and defects modeled as continuous deformations. A practically and theoretically important example is the topologically protected asymmetric transport occurring along interfaces separating two two-dimensional topological insulators (TI) with different topological characteristics. Such systems find wide applications in electronic structures [1, 2], photonics [3, 4, 5], geophysical fluid flows [6], and cold plasma models [7, 8].

The macroscopic description of two-dimensional TIs naturally leads to partial differential equations on the Euclidean plane. The topological classification of such bulk models poses a number theoretical challenges since the Euclidean plane is not compact and the standard notion of Chern numbers used to classify tight-binding and periodic materials [2] or materials displaying a quantum Hall effect with well-defined Landau levels [9] does not apply directly. A number of methods have been developed to regularize these systems by means of a one-point compactification mapping the Euclidean plane $\mathbb{R}^2$ to the Riemann sphere $\mathbb{S}^2 \cong \mathbb{R}^2 \cup$

---

[*]Committee on Computational and Applied Mathematics, University of Chicago, Chicago, IL 60637

[†]Departments of Mathematics and Statistics, Committee on Computational and Applied Mathematics, University of Chicago, Chicago, IL 60637; `guillaumebal@uchicago.edu`

$\{\infty\}$ [5, 10, 11]. $\mathbb{Z}-$valued Chern numbers for Hermitian Hamiltonians in Class A are the only ones considered here [2, 12].

In the classification of the transport asymmetry along interfaces separating different TIs, the notion of bulk phases or bulk invariant is not entirely necessary. One may consider instead the notion of a *bulk difference invariant* (BDI), which is defined in greater generality. BDI were introduced in [13] and further analyzed in [14, 15, 16]. They confirm the intuition that phase differences are more generally defined than differences of absolute phases and were applied in the context of electronic structures to classify interface Hamiltonians modeling bilayer graphene problems [17] and models of Floquet topological insulators [18]. The main technical step in the construction of the BDI is to use a radial compactification of the two Euclidean planes modeling wavenumber of the two phases mapping them to hemispheres of a unit sphere and gluing them continuously along the equator.

The primary usefulness of BDI is their correct prediction of asymmetric edge transport by means of a *bulk-edge correspondence* (BEC), a powerful physical principle in our understanding of topological phases of matter [19, 20, 2, 12, 21]. The BEC states that the excess of number of modes propagating in one direction along the interface with respect to the number propagating in the opposite direction is given by the topological phase difference, i.e., the BDI. Note that the topological protection does not imply that back-scattering is suppressed, but rather that transport in one of the direction is guaranteed even in the presence of strong fluctuations, as a surprising topological obstruction to Anderson localization [22, 23].

To classify asymmetric interface transport, the notion of excess of number of modes is somewhat imprecise unless a complete diagonalization of the interface Hamiltonian is available. A more general notion is the interface current observable σ_I described in (1) below. The interface current, which may be computed by *spectral flow* of an interface Hamiltonian with known diagonalization [16], was introduced in [24] and used in many mathematical derivations of the bulk edge correspondence [12, 25, 26]. In particular, the BEC in [27, 14] takes the form $2\pi\sigma_I = \text{BDI}$ for *elliptic* partial differential operators. Ellipticity is a property of bulk and interface Hamiltonians essentially implying that the energy or frequency is large for wavepackets with large wavenumber, and this uniformly in the position of the wavepacket in the Euclidean plane; see [27, 14, 16] for a more precise definition. Ellipticity is verified by many spin 1/2 Dirac-based models such as the aforementioned applications in [17, 18]. However, they do not hold in many spin 1 type models where three or more bands possibly interact. This has lead to difficulties in establishing the BEC and in fact in various violations of it [28, 29, 30] in models of shallow water equations with discontinuous coefficients or sharp edges.

In the context of photonics and cold plasmas, several difficulties were encountered in establishing or disproving the BEC [21, 31, 32, 33, 34]. In particular, whereas appropriate high-wavenumber regularizations of photonic models led to integer-valued integrals of Berry curvatures, the BEC was not always satisfied. One of the main objectives of this paper is to analyze how the construction of BDI helps to restore the BEC. In particular, we introduce regularizations of photonics and cold plasma models in which the aforementioned gluing of the two phases may be obtained continuously so as do define a *bona fide* Chern number for families of projectors parametrized by the unit sphere.

Our analysis is carried out for a specific 9×9 Hermitian Hamiltonian modeling a linearization of a coupling between a macroscopic electron current with an electromagnetic field

in the presence of a magnetic bias responsible for the non-trivial topological properties. We perform a systematic theoretical analysis of all possible topological phases of the system and all possible frequency gaps shared by two different phases. We then construct BDI for two such phases and show with numerical diagonalization of the corresponding interface Hamiltonian gluing these two phases that the BDI correctly predicts a BEC for most transitions. For phase transitions that are a priori feasible since they share a common insulating gap but involve singular variations in the Hamiltonian, we demonstrate with simple 2×2 systems why the BEC should not be expected to hold. By analogy to electronic structures, the type of singularities we address correspond to Hamiltonians with locally vanishing Fermi velocities. We provide a detailed analysis of why the notion of BEC breaks down in such cases even when the Hamiltonians involve smooth coefficients and no edges.

The rest of the paper is structured as follows. Section 2 recalls the appropriate notions of invariants for two dimensional bulk and interface Hamiltonians in class A, in particular interface current observables, integrals of Berry curvature, Chern numbers obtained by one-point compactification and by radial compactification, and a simple method to compute such integrals theoretically for rotationally symmetric Hamiltonians. Section 2.5 concludes with novel material presenting simple Dirac-type Hamiltonians for which the BEC should not be expected to hold. Section 3 describes our cold plasma model and its topological classification, essentially building on the past works [21, 31, 33, 7, 8]. Our main results are presented in section 4. The central novelty of our analysis is the introduction of high-wavenumber regularizations of the Hamiltonian that differ from those in the aforementioned references and allow us to define *bona fide* integer-valued BDI. Extensive numerical simulations of interface Hamiltonians modeling the spatial transition between different topological phases prove that our BDI is consistent with the BEC in non-singular cases. Additional details on derivations and numerical methods may be found in Appendices.

2   Interface and Bulk invariants

This section summarize the construction and computation of bulk and interface invariants that we will use in the next section. We refer to [2, 12, 5, 16] for additional detail.

We consider continuous Hermitian Hamiltonians H_I acting on vector-valued functions in two space dimensions $(x, y) \in \mathbb{R}^2$ and modeling a smooth transition near the *equator* $\{y = 0\}$ between two topological insulators denoted by constant-coefficient Hamiltonians H^h for $h \in \{N, S\}$. We assume that the coefficients of H_I are given by those of H^N when $y \geq 1$ and by those of H^S when $y \leq -1$. The main example of Hamiltonian considered here is the light-matter interaction system in (12) below.

We use the following notation. We denote by $\mathbf{k} = (k_x, k_y)$ the conjugate (Fourier) variables to (x, y). We denote by Π_j^h or P_j^h families of projectors related to the band structure of H^h. The integrals of Berry curvatures associated to a projector Π are denoted by $\mathcal{C}[\Pi]$. They do not need to be integer-valued. Bona fide integer-valued Chern numbers are systematically denoted by $\mathfrak{C}[\cdot]$. We use $\bar{\alpha}$ to denote complex conjugation of α and A^* to denote Hermitian conjugate of an operator A.

2.1 Interface invariant

A robust and general way to quantify the interface asymmetry is to consider the following interface current observable [12, 25, 16].

Let $P = P(x)$ be a function that depends only the spatial coordinate x with $P(x) = 0$ for $x < x_0 - \delta$ and $P(x) = 1$ for $x > x_0 + \delta$ for some $x_0 \in \mathbb{R}$ and $\delta > 0$. The function $P(x)$ should be interpreted as the observable quantifying the field density in the (right) half-space $x \geq x_0$. Then $i[H, P]$ with $[A, B] = AB - BA$ the standard commutator, may naturally be interpreted as a current operator modeling transfer of field density per unit time across the (thick) vertical line where P transitions from 0 to 1.

The bulk Hamiltonians H^N and H^S are both assumed to be insulators for a frequency or energy interval $[E_0, E_1]$. Any excitation generated in such an interval will therefore be confined to the vicinity of the interface $y \approx 0$ separating the insulators. We define $0 \leq \varphi \in C^\infty(\mathbb{R})$ as a function such that $\varphi(E) = 0$ for $E \leq E_0$ and $\varphi(E) = 1$ for $E \geq E_1$. Thus $\varphi'(H_I)$ defines a density of states of modes that cannot propagate into the N and S bulks.

The expectation value of the current observable $i[H_I, P]$ for a density of states $\varphi'(H_I)$ is then defined as:

$$\sigma_I[H_I] = \text{Tr } i[H_I, P]\varphi'(H_I) \tag{1}$$

assuming that $i[H_I, P]\varphi'(H_I)$ is a trace-class operator. Here, Tr is the standard trace on the Hilbert space $\mathcal{H}$ where H_I is defined. We will refer to σ_I as an interface (current) observable. It is the physical object describing asymmetric transport along an interface, which here is modeled as the $x-$axis.

This observable has been analyzed and related to topological invariants in many settings; see e.g. references in [16]. The computation of the interface current observable is difficult in practice unless the operator H_I may be fully diagonalized; see [16, §3] for a computation using spectral flows, which is how $2\pi\sigma_I$ will be computed numerically in section 4. Its computation is significantly simplified if it may be related to the properties fo the bulk Hamiltonians H^N and H^S. A general principle, the bulk-edge correspondence (BEC) allows one to do so. We first recall the construction of bulk invariants.

2.2 Bulk and Bulk difference invariants (BDI)

We consider two families of self-adjoint Hamiltonians in Fourier variables $H^h(\mathbf{k})$ for $h \in \{N, S\}$ and $\mathbf{k} \in \mathbb{R}^2$ with values in $\mathbb{C}^n \times \mathbb{C}^n$ and assume the following spectral decomposition

$$H^h(\mathbf{k}) = \sum_{j=1}^n \lambda_j^h(\mathbf{k})\Pi_j^h(\mathbf{k})$$

where $\Pi_j^h(\mathbf{k}) = \psi_j^h(\mathbf{k}) \otimes \psi_j^h(\mathbf{k})$ are rank-one projectors and $\lambda_j^h(\mathbf{k})$ are the corresponding eigenvalues. Associated to each (arbitrary-rank) projector family $\mathbb{R}^2 \ni \mathbf{k} \mapsto \Pi(\mathbf{k})$ is the following integral of the associated (Berry) curvature

$$\mathcal{C}[\Pi] = \frac{i}{2\pi} \int_{\mathbb{R}^2} \text{tr}\Pi d\Pi \wedge d\Pi, \qquad d\Pi := \frac{\partial \Pi}{\partial k_x}dk_x + \frac{\partial \Pi}{\partial k_y}dk_y. \tag{2}$$

Here tr stands for standard matrix trace. Because $\mathbb{R}^2$ is not a compact manifold, the above integral is not necessarily a Chern number or necessarily integral-valued.
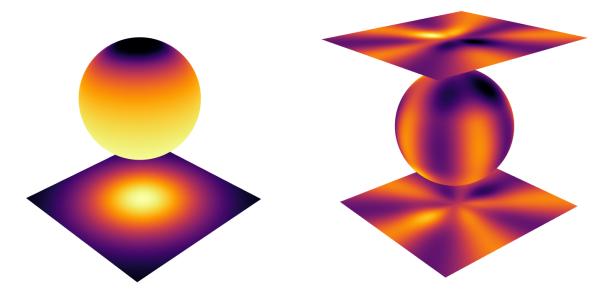
Figure 1: Visual comparison between one-point (left) and radial (right) compactification. On the left the function mapped onto $\mathbb{S}^2$ is continuous due to the limit at infinity being uniform in all directions. Meanwhile on the right two functions are mapped to the upper- and lower-half of $\mathbb{S}^2$ respectively and are glued together along the equator. As long as condition (5) holds the combination is continuous on $\mathbb{S}^2$.

One-point compactification and absolute phase invariants. When the projector family $\Pi(\mathbf{k})$ has a unique limit at the point at infinity $\mathbf{k} = \infty$, i.e., when $\Pi(r\theta) \to \Pi_\infty$ as $r \to \infty$ with Π_∞ independent of $\theta \in \mathbb{S}^1$, we may then project the plane $\mathbb{R}^2$ stereographically onto the Riemann sphere $\mathbb{S}^2$, its one-point compactification. The resulting family of operators on the Riemann sphere is then continuous, in which case we define

$$\mathfrak{C}[\Pi] := \mathcal{C}[\Pi] \in \mathbb{Z} \tag{3}$$

as a *bona fide* Chern number with base manifold the Riemann sphere $\mathbb{S}^2$ [5, 11].

Radial compactification and bulk-difference invariant. In many applications, the family of projectors is not continuous at the point at infinity $\mathbf{k} = \infty$. A radial compactification may be preferred instead.

Assume a spectral gap between levels ℓ and $\ell + 1$ for both $h = N$ and $h = S$, i.e., a frequency interval I_ℓ such that $\lambda_j^h(\mathbf{k}) < I_\ell$ for $h \in N, S$ and $j \leq \ell$ while $\lambda_j^h(\mathbf{k}) > I_\ell$ for $h \in N, S$ and $j \geq \ell + 1$. Associated to the spectral gap are the projectors:

$$P_\ell^h = \sum_{j \leq \ell} \Pi_j^h, \qquad \mathcal{W}_\ell^h := \mathcal{C}[P_\ell^h] = -\mathcal{C}[I - P_\ell^h], \qquad I - P_\ell^h = \sum_{j \geq \ell+1} \Pi_j^h.$$

The total curvature associated to a band may be computed as a sum either over bands below the gap or over bands above the gap. We will use the latter option in section 3. We then

define the bulk-difference invariant for the gap labeled by ℓ:

$$\mathfrak{C}_\ell := \mathfrak{C}[P_\ell^S, P_\ell^N] := \mathcal{W}_\ell^S - \mathcal{W}_\ell^N = \frac{i}{2\pi} \int_{\mathbb{R}^2} \mathrm{tr} P_\ell^S dP_\ell^S \wedge dP_\ell^S - \frac{i}{2\pi} \int_{\mathbb{R}^2} \mathrm{tr} P_\ell^N dP_\ell^N \wedge dP_\ell^N. \quad (4)$$

Provided that we have the following gluing condition

$$\lim_{r\to\infty} P_\ell^N(r\theta) = \lim_{r\to\infty} P_\ell^S(r\theta) \quad \text{for all } \theta \in \mathbb{S}^1, \quad (5)$$

then $\mathfrak{C}_\ell$ is also a *bona fide* Chern number for a family of projectors defined on the sphere $\mathbb{S}^2$. Indeed, we stereographically project P_ℓ^N onto the upper hemisphere of $\mathbb{S}^2$ and P_ℓ^S onto the lower hemisphere of $\mathbb{S}^2$ while the above gluing condition ensures that the family of projectors on $\mathbb{S}^2$ is continuous across the equator. This guarantees that $\mathfrak{C}_\ell \in \mathbb{Z}$, which we call a *Bulk Difference Invariant* (BDI); see Figure 1.

In practice, we often verify the following continuity condition for each band $j \le \ell$,

$$\lim_{r\to\infty} \Pi_j^N(r\theta) = \lim_{r\to\infty} \Pi_j^S(r\theta) \quad \text{for all } \theta \in \mathbb{S}^1.$$

This implies that

$$\mathfrak{C}[\Pi_j^S, \Pi_j^N] = \mathcal{C}[\Pi_j^S] - \mathcal{C}[\Pi_j^N] \in \mathbb{Z}, \qquad \mathfrak{C}[P_\ell^S, P_\ell^N] = \sum_{j \le \ell} \mathfrak{C}[\Pi_j^S, \Pi_j^N],$$

by the (non-trivial) additivity property of Chern numbers.

That the radial compactification is more generally defined than the one-point compactification reflects the fact that topological phase differences are more generally defined than absolute topological phases. In the application to continuous models in photonics and cold plasmas, unperturbed models display behavior of projectors $\Pi(\mathbf{k})$ as $|\mathbf{k}| \to \infty$ that allow for neither one-point nor radial compactification. We will consider several *high-wavenumber regularizations* [5, 21, 31, 32, 33] and show that those regularizations for which BDI can be constructed to correctly predict the presence and number of topologically protected edge states.

2.3 Computation of Chern numbers in isotropic case.

The computation of the above invariants involves integrals of the form $\mathcal{C}[\Pi]$, whether they are integral-valued or not. Computing such integrals analytically is not always straightforward but drastically simplifies in the presence of rotational symmetry. Assume $\Pi(\mathbf{k}) = \psi(\mathbf{k})\psi^*(\mathbf{k})$ a rank-one projector. We then verify that

$$\mathrm{tr}\Pi d\Pi \wedge d\Pi = dA, \qquad A(\mathbf{k}) = (\psi(\mathbf{k}), d\psi(\mathbf{k}))$$

where A is a one-form-$i\mathbb{R}$-valued (Berry) connection assuming $d\psi(\mathbf{k})$ continuously defined. As an application of the Stokes theorem, we thus observe [2, 5, 31] that

$$\mathcal{C}[\Pi] = \frac{i}{2\pi} \Big(\oint_{|\mathbf{k}|\to\infty} A(\mathbf{k}) - \oint_{|\mathbf{k}|\to 0} A(\mathbf{k}) \Big). \quad (6)$$

When $A(\mathbf{k})$ is continuously defined at $\mathbf{k} = 0$, then the above integral over circles with vanishingly small radii converges to 0. However, writing $\mathbf{k} = |\mathbf{k}|e^{i\theta}$ for $\theta \in [0, 2\pi)$, we observe that the above formula remains valid if $\psi(\mathbf{k})$ is (globally) gauge-transformed to, e.g., $e^{im\theta}\psi(\mathbf{k})$. This flexibility proves convenient in practice.

Assume now that the Hamiltonian family is isotropic. Let $\mathbf{k} = ke^{i\theta}$ for $e^{i\theta} \in \mathbb{S}^1$ the unit circle. We assume that
$$H(k\theta) = H(\theta) = U(\theta)H(0)U^*(\theta)$$
for $U(\theta)$ a family of $\mathbb{C}^n-$ unitary transformations. This implies that the branches of spectrum $\lambda_j(\mathbf{k}) = \lambda_j(k)$ are independent of θ and we may choose the eigenvectors $\psi_j(\theta) = U(\theta)\psi_j(0)$.

Isotropy, or invariance by rotation, implies that $U^*(\theta)dU(\theta) = U'(0)d\theta$ is independent of $\theta \in [0, 2\pi)$. In this setting, we thus obtain that

$$\mathcal{C}[\Pi] = i\big[\lim_{k\to\infty}(\psi(k), U'(0)\psi(k)) - \lim_{k\to 0}(\psi(k), U'(0)\psi(k))\big]. \tag{7}$$

In other words, all we need to compute is $\psi(\mathbf{k})$ for $\mathbf{k} = (k, 0)$ with $k = 0$ and $k = \infty$. For the cold plasma application, such computations can be obtained analytically. Explicit expressions for the projectors as $k \to \infty$ are also necessary, for instance in order to verify gluing conditions (5).

2.4   Bulk-Edge Correspondence

The bulk-edge correspondence is a general principle stating that the edge current asymmetry $2\pi\sigma_I$ is related to the bulk invariants by the relation

$$2\pi\sigma_I[H_I] = \mathrm{BDI} = \mathfrak{C}[P_\ell^S, P_\ell^N] \tag{8}$$

where ℓ is a common spectral gap of the bulk Hamiltonians H^h for $h \in \{N, S\}$ and the density φ' appearing in (1) is supported in that common gap. This relation thus implies that the number of edge modes characterized by $2\pi\sigma_I$ is independent of the details of the transition between H^S and H^N.

While natural and ubiquitous in the analysis of topological phases of matter [2, 12], the BEC does not always hold for continuous Hamiltonians. A class of continuous operators for which it is guaranteed to apply is that of *elliptic* operators [13, 16, 14]. Elliptic operators are essentially characterized by singular values $|\lambda_j^h(\mathbf{k})| \to \infty$ as $|\mathbf{k}| \to \infty$ for all branches j and both $h \in \{N, S\}$; see above references.

The operators naturally appearing in shallow water models [6], photonics [5, 32], or biased cold plasmas [35, 33] are not elliptic and it is not always immediate how to naturally regularize them so that they become elliptic. For the well-studied shallow water problem, the BEC is shown to fail in the presence of non-smooth coefficients or boundary conditions [30, 36, 29]. Yet natural elliptic regularizations, for which the BEC holds, may be introduced [13, 16, 14]. This is more difficult to implement in the context of photonics and cold plasma models since the obstruction to ellipticity involves several topologically non-trivial bands. In section 4, we will aim to regularize the Hamiltonians to ensure that we have defined invariants $\mathrm{BDI} = \mathfrak{C}[P_\ell^S, P_\ell^N]$. That (8) still holds in that case will be demonstrated with numerical simulations of $2\pi\sigma_I$ using spectral flow analyses.

To analyze several phase transitions more precisely, we will introduce reduced Hamiltonians as was done in, e.g., [33]. These reduced Hamiltonians model the interaction of two bands, and as such take the form of Dirac-type operators. Reduced interface operators $\tilde{H}_I$ are then either elliptic or singular depending on the phase transition of interest. For elliptic operators, the theory of [27, 14, 16] validates (8). For singular operators, we claim that (8) does not hold as we now demonstrate more precisely.

2.5 Singular Hamiltonians and limitations of the BEC

Reduced Hamiltonian. Consider a bulk Hamiltonian H with two bands associated to eigenvectors $\psi_j(\mathbf{k})$ for $j = 1, 2$ crossing at $\mathbf{k} = 0$ without loss of generality at a frequency $\lambda_1(0) = \lambda_2(0)$. We may then define the reduced Hamiltonian

$$\mathfrak{D}_{ij} = (\psi_i, H\psi_j), \quad 1 \leq i, j, \leq 2.$$

This reduced Hamiltonian takes the form of a two-band Dirac-type operator; see next section and [33]. After formally introducing spatial variations in the constitutive coefficients of the operator, we consider the following model

$$\mathfrak{D}_I = v_x(y)D_x\sigma_1 + \frac{1}{2}\{v_y(y), D_y\}\sigma_2 + [m(y) + \eta\Delta]\sigma_3 + V(y) \tag{9}$$

where $\sigma_{1,2,3}$ are the standard Pauli matrices, $D_{x,y} = -i\partial_{x,y}$, $\{A, B\} = AB + BA$ (ensuring that the above operator is self-adjoint), and where the velocity coefficients $v_{x,y}$, the mass term $m(y)$, and the potential term $V(y)$ are smooth functions allowed to depend on y. Here, η is a small regularization term and Δ is the usual Laplace operator.

When v_x and v_y are constant and $V(y) = 0$, then the BEC (8) holds for the above model [27, 14], of course assuming $\mathfrak{D}^N$ and $\mathfrak{D}^S$ are bulk Hamiltonians with a common gap and φ' in (1) is supported in that gap. The operator is indeed elliptic both before ($\eta = 0$) and after ($\eta \neq 0$) regularization. When $\eta = 0$ and $v_x(y)$ or $v_y(y)$ change signs, however, the operator $\mathfrak{D}_I$ is no longer elliptic. We will call such Hamiltonians singular. These singularities generate violations to the bulk-edge correspondence of a more serious type than for the aforementioned shallow water model [30, 29, 36, 14]. We now illustrate these difficulties.

Elliptic regularization. Assume $m > 0$ constant and $\eta > 0$. Then for $v_{x,y}$ also constant and non-vanishing, the above bulk operator admits a (one-point compactification) bulk invariant [11] given by

$$\mathfrak{C}[\Pi_1] = \text{sign}(v_xv_y)\frac{1}{2}\big(\text{sign}(m) + \text{sign}(\eta)\big) = \text{sign}(v_xv_y).$$

This model results from the continuity of the projector Π_1 at $+\infty$, where Π_1 projects $v_x\xi\sigma_1 + v_y\zeta\sigma_2 + (m - \eta(\xi^2 + \zeta^2))$ onto its one-dimensional negative spectrum.

Consider now a Hamiltonian H_I where $v_y = 1$ and $v_x(y)$ is negative for $y \leq -1$ and positive for $y \geq 1$. In this setting, we can define a difference of bulk invariants

$$2\pi\sigma_I[\mathfrak{D}_I] = \text{BDI} = \mathfrak{C}[\Pi_1^S, \Pi_1^N] = -2.$$

8

The BEC holds for φ' supported in the vicinity of 0, which is a global gap for both phases $h \in \{N, S\}$. This holds since H_I is indeed an elliptic operator for $\eta > 0$ in the sense of [14].

However, in the absence of regularization $\eta = 0$, this operator is clearly not elliptic since a leading term $v_x(y)$ changes signs. The consequences are that the edge modes predicted by the BEC, while indeed present, strongly depend on the regularization. While we do not have an explicit expression for the edge modes of the above model, let us consider the similar Hamiltonian with partial regularization

$$\mathfrak{D}_I = v_x(y)D_x\sigma_1 + D_y\sigma_2 + [m + \eta\partial_x^2]\sigma_3, \quad \hat{\mathfrak{D}}_I = v_x(y)\xi\sigma_1 + D_y\sigma_2 + [m - \eta\xi^2]\sigma_3. \quad (10)$$

The operator $\mathfrak{D}_I$ admits the following spectral decomposition near 0. Define $\mathfrak{a} = \partial_y + \xi\varphi(y)$. Then for $\mathfrak{a}\psi_1 = 0$ and $\psi_2 = 0$, we obtain that $\psi = (\psi_1, \psi_2)^T$ solves $\hat{\mathfrak{D}}_I\psi = E(\xi)\psi$ with $E(\xi) = (m - \eta\xi^2)$ when $\xi > 0$. For $\xi < 0$, we similarly obtain $\mathfrak{a}^*\psi_2 = 0$ for $\psi_1 = 0$ and $E(\xi) = -(m - \eta\xi^2)$ when $\xi > 0$. This implies the presence of edge states at energy $E = 0$ for wavenumbers $\xi = \pm(m/\eta)^{\frac{1}{2}}$ with edge modes concentrated near $y = 0$ by $e^{-|\xi|\Phi(y)}$ where we defined $\Phi(y) = \int_0^y \varphi(z)dz$.

These edge modes, while predicted by theory, occur for wavenumbers $\mathbf{k}$ of order $\eta^{-\frac{1}{2}} \gg 1$ which may not be physically present when dissipative effects are accounted for. Moreover, such modes are unstable against perturbations of the regularization: changing $\eta > 0$ to $\eta < 0$ implies

$$2\pi\sigma_I[\mathfrak{D}_I] = \mathrm{BDI} = \mathfrak{C}[\Pi_1^S, \Pi_1^N] = 0.$$

Consider again (10) now with $\eta < 0$. Then $\hat{\mathfrak{D}}_I\psi = \psi$ indeed implies that $((m + \eta\xi^2)^2 + \mathfrak{a}\mathfrak{a}^*)\psi_2 = E^2\psi_2$ while $((m + \eta\xi^2)^2 + \mathfrak{a}^*\mathfrak{a})\psi_1 = E^2\psi_1$ implying that $\hat{\mathfrak{D}}_I$ for each ξ, and hence $\mathfrak{D}_I$, is gapped in $(-m, m)$. This is consistent with the above prediction $\mathrm{BDI} = 0$.

Singular Hamiltonian I. Consider a slight modification of the above operator with $\eta = 0$:

$$\tilde{\mathfrak{D}}_I = e^{-i\theta(y)\sigma_2}H_I e^{i\theta(y)\sigma_2}, \quad \mathfrak{D}_I = v_x(y)D_x\sigma_1 + D_y\sigma_2 + m\sigma_3,$$

where $v_x(y) = 1$ for $y \geq 1$ and $v_x(y) = -1$ for $y \leq -1$ and where $\theta(y)$ is a smooth function such that $\theta(y) = 0$ for $y \geq 1$ and $\theta(y) = \frac{\pi}{2}$ for $y \leq -1$. We observe that $e^{\pm i\frac{\pi}{2}\sigma_2} = \pm i\sigma_2$. Thus

$$\tilde{\mathfrak{D}}^N = D_x\sigma_1 + D_y\sigma_2 + m\sigma_3, \qquad \tilde{\mathfrak{D}}^S = D_x\sigma_1 + D_y\sigma_2 - m\sigma_3.$$

No bulk phases may be obtained for the unregularized $\tilde{H}^h$ for $h \in \{N, S\}$ but a BDI may be defined [16, 14] as

$$\mathfrak{C}[\tilde{\Pi}_1^S, \tilde{\Pi}_1^N] = \mathrm{BDI} = -1.$$

The presence of $\theta(y) \neq 0$ is there to ensure that $\tilde{\Pi}_1^S$ and $\tilde{\Pi}_1^N$ satisfy the gluing condition (5), which would not hold for $\theta \equiv 0$. Now, $\tilde{\mathfrak{D}}_I$ is unitarily equivalent to $\mathfrak{D}_I$, which in Fourier variables is $\hat{\mathfrak{D}}_I = v_x(y)\xi\sigma_1 + D_y\sigma_2 + m\sigma_3$. This operator, as in (10), is however gapped in $(-m, m)$. We are thus in a situation where

$$2\pi\sigma_I[\tilde{\mathfrak{D}}_I] = 0, \qquad \mathfrak{C}[\tilde{\Pi}_1^S, \tilde{\Pi}_1^N] = \mathrm{BDI} = -1$$

in complete contradiction of the BEC. The change of sign of $v_x(y)$ in a leading term of the Dirac operator is a strong violation of ellipticity. The above model is relevant in some phase transitions considered in the next section.

Singular Hamiltonian II. Consider the above Hamiltonian with $\eta = 0$ and with $v_x(y) = y$ while $v_y(y) = m(y) = |y|$. These functions could be assumed smoother without affecting the results we obtain. This highly singular Hamiltonian, with the same bulk properties $BDI = -1$ as above, also finds applications in the analysis of some phase transitions in the next section. We now show that the whole line $\mathbb{R}$ belongs to the essential spectrum of $\mathfrak{D}_I$ so that $\sigma_I[\mathfrak{D}_I]$ is not defined as $i[\mathfrak{D}_I, P]\varphi'(\mathfrak{D}_I)$ is not trace-class and (8) cannot possibly hold.

Consider the standard change of variables $\mathbb{R}_+ \ni y = e^z$ for $z \in \mathbb{R}$ so that $dy = ydz$. Using the corresponding map $\varphi(z) = y^{\frac{1}{2}}\psi(z)$, we observe that $\|\psi\| = \|\varphi\|$ so that the map is unitary and that moreover $\mathfrak{D}_I\psi = E\psi$ is equivalent to

$$\mathfrak{D}_z\varphi(z) = (e^z\xi\sigma_1 + D_z\sigma_2 + e^z\sigma_3)\varphi(z) = E\varphi(z).$$

The above shows that $\mathfrak{D}_I$ and $\mathfrak{D}_z$ are unitarily equivalent. We now observe that $\mathbb{R}$ belongs to the spectrum of $\mathfrak{D}_z$ for each $\xi \in \mathbb{R}$. Indeed, let $\chi(z) \in C_c^\infty(\mathbb{R})$ be such that $\int_{\mathbb{R}} \chi^2(z)dz = 1$ and $\int_{\mathbb{R}}(\chi')^2(z)dz < \infty$ and such that $\chi(z) = 0$ for $z \geq -1$ and $z \leq -3$. We next define the sequence

$$\varphi_N(z) = \frac{1}{\sqrt{N}}\chi(\frac{z}{N})e^{-iEz}\frac{1}{\sqrt{2}}\begin{pmatrix} 1 \\ i \end{pmatrix}.$$

We observe that

$$(\mathfrak{D}_z - E)\varphi_N(z) = e^{-N}r_N(z) + \frac{1}{N}\chi'(\frac{z}{N})s_N(z)$$

with r_N square integrable and s_N bounded. This implies that φ_N is a Weyl sequence normalized in $L^2(\mathbb{R})$ and without accumulation point as $N \to \infty$. This further implies that

$$\psi_N(z) = y^{-\frac{1}{2}}\varphi_N(\ln y)$$

is also a Weyl sequence, also without accumulation points as supports are disjoint for large, sufficiently different, values of N. Standard results in spectral theory [37, Chapter 2] show that $\mathbb{R}$ is in the essential spectrum of H with Weyl sequence independent of ξ, which heuristically looks like a continuum of flat bands. Clearly, for φ' supported near the origin, then $i[H, P]\varphi'(H)$ is not trace-class so that σ_I cannot be defined. Note that these functions can be extended by 0 for $y < 0$ while another set of Weyl sequences can be constructed with support in $y < 0$.

This gives an example where $BDI = -1$ does not predict the edge mode structure. In fact, we have a continuum of modes that decay like $|y|^{-\frac{1}{2}}$ and hence while localized near the interface $y = 0$ cannot really be considered as edge modes. The linear vanishing of the Fermi velocity creates singular operators for which the BEC is incorrect. This highly singular Hamiltonian essentially ensures that the half spaces $y > 0$ and $y < 0$ are independent. The bulk-edge correspondence, implying that edge states are independent of the transition between the bulk phases, cannot possibly hold.

3   Topological phases in cold plasma model

3.1   Cold plasma Hamiltonian model

We now focus on the analysis of a continuous Hamiltonian that finds applications in the modeling of biased cold plasmas and photonic materials [5, 38, 33]. We start with the following linearized light-matter interaction system

$$
\begin{aligned}
m_e \frac{\partial v}{\partial t} &= q_e(E + v \times B_i) \\
c^2 \nabla \times B &= \frac{n_e q_e v}{\epsilon_0} + \frac{\partial E}{\partial t} \\
\nabla \times E &= -\frac{\partial B}{\partial t},
\end{aligned}
\tag{11}
$$

where $v(\mathbf{r})$ denotes electron current and $(E(\mathbf{r}), B(\mathbf{r}))$ the electromagnetic field at $\mathbb{R}^3 \ni \mathbf{r} = (x, y, z)$. Also, (m_e, q_e, ϵ_0) are fundamental constants while $B_i = B_0(x, y)\hat{e}_z$ and $n_e = n_e(x, y)$ are given bias magnetic field and plasma density, respectively. Assuming that the Lorentz force depends only on the incident magnetic field amounts to assuming that to 0-th order the electron velocity is 0, $v^{(0)} = 0$, which is the main assumption of the cold plasma model. See [39] for more discussion and a derivation as a limit of kinetic theory of hot plasma. We thus assume the system invariant by translations along the z variables so that the dual variable k_z is a good quantum number that becomes a parameter in the system.

We introduce the rescaled quantity and change of variables

$$
\Omega(x, y) = \frac{q_e B_0(x, y)}{m_e}, \quad \omega_p(x, y) = \sqrt{\frac{n_e(x, y) q_e^2}{m_e \epsilon_0}}, \quad cB \to B, \quad v(t, x, y)\sqrt{\frac{m_e n_e(x, y)}{\epsilon_0}} \to v(t, x, y)
$$

where $\Omega(x, y)$ is the cyclotron frequency and $\omega_p(x, y)$ the plasma frequency, to obtain the Hamiltonian system of 9×9 equations for $\psi = (v, E, H)^T$:

$$
i\partial_t \psi = H_I \psi, \qquad H_I := \begin{pmatrix} i\Omega(x, y)\hat{e}_z \times & -i\omega_p(x, y) & 0 \\ i\omega_p(x, y) & 0 & i\nabla \times \\ 0 & -i\nabla \times & 0 \end{pmatrix}.
\tag{12}
$$

We denote by H_I this Hamiltonian to include a transition between different insulating bulks. In this paper, we assume all parameters of the system independent of x and to be continuous in y. The above Hamiltonian defines the constant coefficient Hamiltonians H^N when $y \gg 1$ and H^S when $y \ll 1$. In the dual Fourier variables $\boldsymbol{k} = (\mathbf{k}, k_z)$ to $\mathbf{r}$, these operators take the form for each fixed $k_z \in \mathbb{R}$ of the family

$$
\mathbb{R}^2 \ni \mathbf{k} \mapsto H(\mathbf{k}) = \begin{pmatrix} i\Omega(k)\hat{e}_z \times & -i\omega_p(k) & 0 \\ i\omega_p(k) & 0 & -\boldsymbol{k} \times \\ 0 & \boldsymbol{k} \times & 0 \end{pmatrix}, \qquad u \times := \begin{pmatrix} 0 & -u_z & u_y \\ u_z & 0 & -u_x \\ -u_y & u_x & 0 \end{pmatrix}.
\tag{13}
$$

While the coefficients (Ω, ω_p) are constant in the model, we will assume the presence of regularization mechanisms to suppress unwanted phenomena as $\mathbf{k} \to \infty$. This is anticipated in the above expressions where $\Omega(k)$ and $\omega_p(k)$ are allowed to depend on $k = |\mathbf{k}|$.

Our objective in this section is to associate interface invariants to H_I and bulk difference invariants to $H(\mathbf{k}) = H(\mathbf{k}; \Omega, \omega_p, k_z)$ as the parameters (k_z, Ω, ω_p) vary.

3.2   Symmetries of the problem

We first analyze the spectral properties of the bulk Hamiltonians $H(\mathbf{k}) = H(\mathbf{k}; \Omega, \omega_p, k_z)$.

Invariance by rotation.   We decompose $\mathbf{k} = ke^{i\theta}$ for $\theta \in [0, 2\pi)$ and introduce $R(\theta)$ be the family of orthogonal operators

$$R(\theta) = \begin{pmatrix} \cos\theta & -\sin\theta & 0 \\ \sin\theta & \cos\theta & 0 \\ 0 & 0 & 1 \end{pmatrix} \quad \text{such that} \quad \boldsymbol{k} = R(\theta)(k, 0, k_z)^T.$$

Using the notation $H(\theta) = H(ke^{i\theta})$ and defining $\mathrm{R}(\theta) = \mathrm{Diag}(R(\theta), R(\theta), R(\theta))$, we observe that

$$\mathrm{R}^*(\theta)H(\theta)\mathrm{R}(\theta) = H(0). \tag{14}$$

This is a direct consequence of the fact that $\boldsymbol{k}\times$ and $e_z\times$ satisfy the above invariance. This shows that the spectrum of the family $H(\mathbf{k})$ is invariant by rotation parametrized by $\theta \in [0, 2\pi)$. Moreover, the transformation of eigenvectors is given by $\psi(\theta) = \mathrm{R}^*(\theta)\psi(0)$ and (7) applies with $U'(0) = \mathrm{R}'(0)$.

Discrete symmetries.   Define the parity operator

$$\Gamma_P(\theta) = \mathrm{Diag}(S(\theta), -S(\theta), -S(\theta)), \ \ S(\theta) = \begin{pmatrix} \cos(2\theta)\sigma_3 + \sin(2\theta)\sigma_1 & 0 \\ 0 & 1 \end{pmatrix} = R(\theta)S(0)R^*(\theta).$$

We observe that $\Gamma_P(\theta) = \Gamma_P^*(\theta)$ and $\Gamma_P^2(\theta) = I_9$. Moreover, we have the parity invariance

$$\Gamma_P(\theta)H(\theta)\Gamma_P^*(\theta) = -H(\theta) \tag{15}$$

This shows that $H(\theta)$ is unitarily equivalent to $-H(\theta)$. This parity relation implies that the spectrum of H is symmetric about 0. Moreover, for eigenvalues different from 0, their corresponding eigenvectors $\psi(\theta)$ and $\Gamma_P^*(\theta)\psi(\theta)$ are orthogonal.

This result comes from an explicit calculation where k_y is first sent to 0 by rotation and then the observation that $S(0)k \times S(0) = -k\times$ when $k_y = 0$. We observe for the same reason that $S(\theta)\hat{e}_z \times S(\theta) = -\hat{e}_z$.

Defining the operators $\Gamma_\Omega = \mathrm{Diag}(I_3, -I_3, I_3)$ and $\Gamma_k = \mathrm{Diag}(I_3, I_3, -I_3)$, we observe that

$$\Gamma_\Omega H(\theta; \Omega)\Gamma_\Omega = -H(\theta; -\Omega), \qquad \Gamma_k H(\theta; k)\Gamma_k = H(\theta; -k). \tag{16}$$

Since $\omega_p > 0$ physically, we do not consider the case $\omega_p < 0$.

Combining the two preceding results shows that the spectrum is invariant under $\Omega \to -\Omega$:

$$\tilde{\Gamma}_P(\theta) H(\theta, \Omega) \tilde{\Gamma}_P(\theta) = H(\theta, -\Omega), \qquad \tilde{\Gamma}_P(\theta) = \tilde{\Gamma}_P^*(\theta) := \Gamma_P(\theta)\Gamma_\Omega. \tag{17}$$

For $H(\theta, \Omega)\psi = \omega\psi$, we thus obtain that $H(\theta, -\Omega)[\Gamma_P^*(\theta)\Gamma_\Omega\psi] = \omega[\Gamma_P^*(\theta)\Gamma_\Omega\psi]$. Note that $\tilde{\Gamma}_P(\theta) = \mathrm{Diag}(S(\theta), S(\theta), -S(\theta))$.

Similarly, defining $\tilde{\Gamma}_k = \Gamma(k)\mathrm{R}(\pi)$, we observe that

$$\tilde{\Gamma}_k H(\mathbf{k}; k_z) \tilde{\Gamma}_k = H(\mathbf{k}; -k_z) \tag{18}$$

so that for instance $H(k_z)\psi = \omega\psi$ implies that $H(-k_z)[\tilde{\Gamma}_k\psi] = \omega[\tilde{\Gamma}_k\psi]$.

Note that $\bar{H}(k) = -H(-k)$ as one readily verifies so that $\Gamma_k \bar{H}(k)\Gamma_k = -H(k)$. Note also that $\bar{\psi}(k) = \psi(-k)$ since H_I has real-valued coefficients in the physical variables. This imposes that $H(k)(\Gamma_k\psi(-k)) = -\omega(k)(\Gamma_k\psi(-k))$ also implying that the spectrum of H is symmetric about 0 as shown in, e.g., [33]. The above derivation defines a precise unitary equivalence between $H(k)$ and $-H(k)$ via $\Gamma_P(\theta)$.

3.3 Topological phases

We saw in the preceding section that all we needed to compute integrals as in (2) were the eigenvectors $\psi(k, 0)$ for $k \in \mathbb{R}_+$. In order to be able to apply Stokes formula leading to (6) we make the assumption that the branches $k \to \lambda_j(k)$ do not cross. We do not have a theoretical justification for this absence of crossing for $0 < k < \infty$ beyond extensive numerical simulations. In fact, branches do cross at $k = 0$, $k = \infty$, $k_z = 0$, and $\Omega = 0$. This is the reason for the existence of several phases of matter for the cold plasma model, and why first we consider only strictly positive (Ω, ω_p, k_z) and treat the $k_z = 0$ and $\Omega = 0$ cases separately.

By parity invariance, $\omega = 0$ is always an eigenvalue of $H(\mathbf{k})$, which we verify is associated to $\psi_0 = (0, 0, \boldsymbol{k}/|\boldsymbol{k}|)$.

We first consider the rest of the diagonalization of $H(k = 0)$. We assume all coefficients (Ω, ω_p, k_z) strictly positive. By parity, there are four positive eigenvalues and four negative eigenvalues. The four positive eigenvalues are denoted by $(\omega_p, \omega_{L-}, \omega_R, \omega_{L+})$.

Indeed we verify that $\omega = \omega_p$ is always an eigenvalue associated to the eigenvector $\Psi_p = 2^{-\frac{1}{2}}(\hat{e}_z, i\hat{e}_z, 0)^T$. The other eigenvalues are the positive solutions of two cubic equations given explicitly by

$$k_z^2 = \omega_R^2 - \frac{\omega_p^2 \omega_R}{\omega_R + \Omega}, \qquad k_z^2 = \omega_L^2 - \frac{\omega_p^2 \omega_L}{\omega_L - \Omega}. \tag{19}$$

Associated to these eigenvalues are the eigenvectors, up to normalizing constants c:

$$\Psi_{L-} = c \begin{pmatrix} i\frac{\omega_p}{\Omega - \omega_{L-}}\hat{e}_+ \\ \hat{e}_+ \\ -i\frac{k_z}{\omega_{L-}}\hat{e}_+ \end{pmatrix}, \; \Psi_R = c \begin{pmatrix} -i\frac{\omega_p}{\Omega + \omega_R}\hat{e}_- \\ \hat{e}_- \\ i\frac{k_z}{\omega_R}\hat{e}_- \end{pmatrix}, \; \Psi_{L+} = c \begin{pmatrix} i\frac{\omega_p}{\Omega - \omega_{L+}}\hat{e}_+ \\ \hat{e}_+ \\ -i\frac{k_z}{\omega_{L+}}\hat{e}_+ \end{pmatrix}, \; \hat{e}_\pm = \frac{1}{\sqrt{2}} \begin{pmatrix} 1 \\ \pm i \\ 0 \end{pmatrix}.$$

13

We always have $0 < \omega_{L-} < \omega_R < \omega_{L+}$ (see Appendix F for details) but the relation among the other eigenvalues is not fixed and in fact defines different topological phases.

These phase transitions occur as in [33] for the values

$$0 < \frac{\omega_\pm}{|\Omega|} = \frac{1}{2}\left(\sqrt{\left(\frac{k_z}{\Omega}\right)^4 + 4\left(\frac{k_z}{\Omega}\right)^2} \pm \left(\frac{k_z}{\Omega}\right)^2\right) \tag{20}$$

where $\omega_\pm$ are defined as the transitions $\omega_- = \omega_p = \omega_{L-}$ and $\omega_+ = \omega_p = \omega_R$. We also note that ω_- is defined only for under-dense plasma where $\omega_p < \Omega$ while ω_+ is defined for all values of (Ω, ω_p, k_z); see Figure 2.
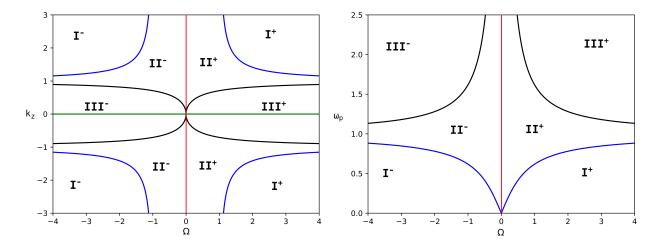

Figure 2: Topological phases as in the Ω, k_z plane for $\omega_p = 1$ (left) and Ω, ω_p plane for $k_z = 1$ (right). Black lines indicate the $k_z = k_+$ and $\omega_p = \omega_+$ boundaries, blue the $k_z = k_-$ and $\omega_p = \omega_-$ boundaries, and red $\Omega = 0$ boundary. The green line on the left represents phase IV$^\pm$ ($k_z = 0$).

This allows us to define 6 distinct *topological phases*. The phases I$^+$, II$^+$, and III$^+$ are defined for

$$\begin{aligned}
\text{I}^+ : &\quad 0 < \omega_p < \omega_- < \omega_{L-} \\
\text{II}^+ : &\quad 0 < \omega_{L-} < \omega_- < \omega_p < \omega_+ < \omega_R \\
\text{III}^+ : &\quad 0 < \omega_{L-} < \omega_- < \omega_R < \omega_+ < \omega_p < \omega_{L+}.
\end{aligned}$$

The phase I$^+$ is defined only for under-dense plasmas. The phases I$^-$, II$^-$, and III$^-$ are defined for $\Omega < 0$ by the same constraints that $0 < \omega_p$ is respectively the smallest, second smallest, or second largest (strictly positive) eigenvalue. The case $\Omega = 0$ is singular and so the above six phases are characterized by different invariants.

Eigenvectors as $k \to \infty$. In order to apply (7), we need to evaluate the behavior as $k \to \infty$ of the above eigenvectors. We do not have explicit expressions for these eigenvectors for arbitrary values of $0 < k < \infty$. For $k \to \infty$, we obtain for the four eigenvectors associated

14

to $\omega_1 = 0$, $\omega_2 = \sqrt{\omega_p^2 + \Omega^2}$, $\omega_3 = k + o(1)$ and $\omega_4 = k + o(1)$, up to normalization by:

$$\Psi_1 = \begin{pmatrix} \frac{-\hat{e}_2}{\sqrt{1+\sigma^2}} + i\hat{e}_3 \\ \frac{-\sigma\hat{e}_1}{\sqrt{1+\sigma^2}} \\ 0 \end{pmatrix}, \quad \Psi_2 = \begin{pmatrix} \frac{-\sigma\hat{e}_2}{\sqrt{1+\sigma^2}} - i\hat{e}_1 \\ \frac{\hat{e}_1}{\sqrt{1+\sigma^2}} \\ 0 \end{pmatrix}, \quad \Psi_3 = \begin{pmatrix} 0 \\ \hat{e}_3 \\ -\hat{e}_2 \end{pmatrix}, \quad \Psi_4 = \begin{pmatrix} 0 \\ \hat{e}_2 \\ \hat{e}_3 \end{pmatrix}, \qquad (21)$$

where we have defined $\sigma = |\Omega|/\omega_p$ and assumed $k_x = 0$. Expressions for arbitrary $\mathbf{k}$ can be obtained by applying $R(\theta)^*$ (see Appendix F for details) but since rotations in $\mathbf{k}$ are unitarily equivalent the above vectors are sufficient to calculate bulk- or bulk-difference invariants. Similar expressions may be obtained for $\Omega < 0$ using (17).

Using (7) with $U'(0) = R'(0) = \mathrm{Diag}(J, J, J)$ where $J = \mathrm{Diag}\left(\begin{smallmatrix} 0 & -1 \\ 1 & 0 \end{smallmatrix}\right), 0) = \hat{e}_z \times$, we deduce the results gathered in Table 1.

Phase	$\mathcal{C}_1$	$\mathcal{C}_2$	$\mathcal{C}_3$	$\mathcal{C}_4$	Phase	$\mathcal{C}_1$	$\mathcal{C}_2$	$\mathcal{C}_3$	$\mathcal{C}_4$
I^+	0	$\frac{\sigma}{\sqrt{\sigma^2+1}} - 1$	1	-1	I^-	0	$\frac{-\sigma}{\sqrt{\sigma^2+1}} + 1$	-1	$+1$
II^+	-1	$\frac{\sigma}{\sqrt{\sigma^2+1}}$	1	-1	II^-	1	$\frac{-\sigma}{\sqrt{\sigma^2+1}}$	-1	$+1$
III^+	-1	$1 + \frac{\sigma}{\sqrt{\sigma^2+1}}$	0	-1	III^-	1	$-1 - \frac{\sigma}{\sqrt{\sigma^2+1}}$	0	$+1$
IV^+	0	$1 + \frac{\sigma}{\sqrt{\sigma^2+1}}$	0	-1	IV^-	0	$-1 - \frac{\sigma}{\sqrt{\sigma^2+1}}$	0	$+1$

Table 1: Value of the curvature integrals for the six phases $\mathrm{I}^\pm, \mathrm{II}^\pm, \mathrm{III}^\pm$ and the two phases $\mathrm{IV}^\pm$ corresponding to $k_z = 0$ treated in section 3.4 below.

We observe, as in [33], that these curvature integrals are not always integers. This reflects the fact that $\mathbb{R}^2$ is not a compact manifold and that the projectors Π_j^h do not have a unique value at ∞. Indeed, $\psi(\theta) = R(\theta)\psi_0$ in general has explicit dependence in θ.

3.4 The case $k_z = 0$

The Hamiltonian family $H(\mathbf{k})$ belongs to the same phase ($\mathrm{III}^\pm$ depending on the sign of Ω) for all $|k_z| \ll 1$; note also the unitarily equivalence in (18). However, the case $k_z = 0$ is singular and defines different topological phases since Transverse Magnetic (TM) and Transverse Electric (TE) modes are no longer coupled [5, 31, 40]. We may indeed introduce in the Fourier variables

$$H_{TM} = \begin{pmatrix} 0 & i\Omega & -i\omega_p & 0 & 0 \\ -i\Omega & 0 & 0 & -i\omega_p & 0 \\ i\omega_p & 0 & 0 & 0 & -k_y \\ 0 & i\omega_p & 0 & 0 & k_x \\ 0 & 0 & -k_y & k_x & 0 \end{pmatrix}, \quad H_{TE} = \begin{pmatrix} 0 & -i\omega_p & 0 & 0 \\ i\omega_p & 0 & k_y & -k_x \\ 0 & k_y & 0 & 0 \\ 0 & -k_x & 0 & 0 \end{pmatrix}, \qquad (22)$$

where H_{TM} acts on $(v_x, v_y, E_x, E_y, B_z)^T$ while H_{TE} acts on $(v_z, E_z, B_x, B_y)^T$. These Hamiltonians are invariant by a reduction of R($\mathbf{k}$) to the appropriate components and we may assume that $\mathbf{k} = (k, 0)$. We find that the eigenvalues of H_{TE} are given by $\check{\omega}_{1,2,3,4} = (-\sqrt{k^2 + \omega_p^2}, 0, 0, \sqrt{k^2 + \omega_p^2})$. We verify that all curvature integrals $\mathcal{C}[\Pi_j]$ associated with their eigenvectors vanish; in particular $\mathcal{C}_{1,3} = 0$. Due to the fact that the curvature integrals are distinct from phase III$^\pm$, to which $k_z = 0$ would belong otherwise, but still non-trivial, we denote a separate phase IV$^\pm$ for the $k_z = 0$ case for $\Omega > 0$ and $\Omega < 0$ respectively. In particular note that TE modes acquire a non-trivial topological branch $\mathcal{C}_1 \neq 0$ only after coupling with TM modes.

The eigenvalues of H_{TM} are given by $\tilde{\omega}_{-1,-2} = -\tilde{\omega}_{1,2}$ and

$$\tilde{\omega}_{0,1,2} = \left(0, \frac{1}{2}\left(k^2 + \omega_h^2 - \sqrt{(k^2 - \Omega^2)^2 + 4\omega_p^2\Omega^2}\right), \frac{1}{2}\left(k^2 + \omega_h^2 + \sqrt{(k^2 - \Omega^2)^2 + 4\omega_p^2\Omega^2}\right)\right)$$

where $\omega_h^2 = 2\omega_p^2 + \Omega^2$. If $\omega_{0,1,2,3,4}$ denote the nonnegative eigenvalues of the original 9×9 system, then we verify that $\omega_{0,1,2,3,4} = (0, \check{\omega}_1, \tilde{\omega}_1, \check{\omega}_2, \tilde{\omega}_2)$. The numbers $\mathcal{C}_{2,4}$ in Table 1 are identical in phases III$^\pm$ and IV$^\pm$.

3.5 Reduced models and Dirac Hamiltonians

The first and second spectral bands cross $\omega_1(k = 0) = \omega_2(k = 0)$ at the value ω_-. Similarly the second and third spectral bands cross $\omega_2(k = 0) = \omega_3(k = 0)$ at the value ω_+. Following [33] and the reduction introduced in section 2.5, we derive the corresponding Dirac operators for both $\Omega > 0$ and $\Omega < 0$.

Crossing near ω_- frequency. The regime $|\omega_p - \omega_-| \ll 1$ and $|\mathbf{k}| \ll 1$ is characterized by two nearby bands (ω_1, ω_2) that are isolated from the rest of the Hamiltonian. Following [33], we project H onto the span of $(\Psi_1(0), \Psi_2(0))$ to obtain the following reduced Hamiltonian $\mathfrak{D}_{ij} = \Psi_i^* H \Psi_j$ given by

$$\mathfrak{D} = \omega_- + \begin{pmatrix} \tilde{\omega}_p & \frac{ik_x - k_y}{\alpha} \\ \frac{-ik_x - k_y}{\alpha} & \frac{-2\beta}{\alpha^2}\tilde{\omega}_p \end{pmatrix} = \left(\omega_- + (\frac{1}{2} - \frac{\beta}{\alpha^2})\tilde{\omega}_p\right) - \frac{k_y}{\alpha}\sigma_1 - \frac{k_x}{\alpha}\sigma_2 + (\frac{1}{2} + \frac{\beta}{\alpha^2})\tilde{\omega}_p\sigma_3, \quad (23)$$

where $\tilde{\omega}_p = \omega_p - \omega_-$ and $\alpha^2 = 4 + 3(\frac{k_z}{\Omega})^2 - \frac{k_z}{\Omega}\sqrt{(\frac{k_z}{\Omega})^2 + 4}$ while $\beta = \frac{k_z}{\Omega}(\sqrt{(\frac{k_z}{\Omega})^2 + 4} - \frac{k_z}{\Omega}) = 2\omega_-/\Omega$. Here, we assume $\Omega > 0$.

The case $\tilde{\omega}_p < 0$ corresponds to phase I$^+$ while $\tilde{\omega}_p > 0$ (not too large) corresponds to phase II$^+$. The reduced interface operator $\mathfrak{D}_I$ with $\tilde{\omega}_p = \gamma y$ thus acts as a transition from $\mathfrak{D}^S$ in phase I$^+$ to $\mathfrak{D}^N$ in phase II$^+$.

Because $\frac{1}{2} - \frac{\beta}{\alpha^2} < \frac{1}{2} + \frac{\beta}{\alpha^2}$, we deduce that $\mathfrak{D}_I$ is an *elliptic* operator in the sense of [16, 14].

Crossing near ω_- frequency for $\Omega < 0$. We now consider the same regime $|\omega_p - \omega_-| \ll 1$ and $|\mathbf{k}| \ll 1$ but with now $\Omega < 0$.

The symmetry (17) implies that $H[-\Omega] = \tilde{\Gamma}_P H[\Omega]\tilde{\Gamma}_P$. We observe that likewise projecting H onto $\tilde{\Gamma}_P\Psi_1(k = 0)$ and $\tilde{\Gamma}_P\Psi_2(k = 0)$, yields, for an appropriate choice of phases in

σ_1, σ_2:

$$\mathfrak{D}[-\Omega] = \left(\omega_- + (\frac{1}{2} - \frac{\beta}{\alpha})\tilde{\omega}_p\right) - \frac{k_y}{\alpha}\sigma_1 + \frac{k_x}{\alpha}\sigma_2 + (\frac{1}{2} + \frac{\beta}{\alpha})\tilde{\omega}_p\sigma_3. \qquad (24)$$

See Appendix D for details. In other words, $\Omega \to -\Omega$ may be represented as the change of orientation $k_x \to -k_x$.

Crossing near ω_+ frequency. A similar calculation involving the projection of H onto the span of $(\Psi_2(0), \Psi_3(0))$ for ω_p near the band crossing ω_+ reveals the following reduced Hamiltonian:

$$\mathfrak{D}_+ = \omega_+ + \begin{pmatrix} \tilde{\omega}_p & \frac{k_y + ik_x}{\alpha} \\ \frac{k_y - ik_x}{\alpha} & \frac{2\beta}{\alpha^2}\tilde{\omega}_p \end{pmatrix} = \left(\omega_- + (\frac{1}{2} + \frac{\beta}{\alpha^2})\tilde{\omega}_p\right) + \frac{k_y}{\alpha}\sigma_1 - \frac{k_x}{\alpha}\sigma_2 + (\frac{1}{2} - \frac{\beta}{\alpha^2})\tilde{\omega}_p\sigma_3, \quad (25)$$

where now $\alpha^2 = 4 + 3(\frac{k_z}{\Omega})^2 + \sqrt{(\frac{k_z}{\Omega})^4 + 4(\frac{k_z}{\Omega})^2}$ and $\beta = \frac{k_z}{|\Omega|}(\sqrt{(\frac{k_z}{\Omega})^2 + 4} + \frac{k_z}{|\Omega|}) = 2\omega_+/|\Omega|$. Now because $(\frac{1}{2} + \frac{\beta}{\alpha^2}) > (\frac{1}{2} - \frac{\beta}{\alpha^2})$ we observe that ω_+ is no longer in a spectral gap. The spectral gaps in phases II$^+$ and phases III$^+$ do not overlap, which makes it impossible to have a well defined interface current observable σ_I in (1) in that setting.

4 BDI and Edge States: Main results

Edge states typically appear at interfaces separating insulators in different phases. This requires identifying global spectral gaps that are shared by the two insulators and defining bulk Hamiltonians H^N and H^S with coefficients (Ω^N, ω_p^N) and (Ω^S, ω_p^S) that place H^N and H^S in different phases according to Table 1.

Since the smallest positive eigenvalue converges to 0 and the third largest positive eigenvalue tends to infinity as $k \to \infty$, the only possible spectral gaps are between ω_1 and ω_2 (denoted below by $\ell = 1$) or between ω_2 and ω_3 (denoted below by $\ell = 2$). Such gaps indeed occur for a range of parameters [7].

Once such transitions are identified, we wish to assign a topological invariant to the interface Hamiltonian and verify whether the BEC (8) applies. This requires that we be able to construct Chern numbers, either via a one-point compactification of $\mathbb{R}^2$ or via a radial compactification of two copies of $\mathbb{R}^2$ as recalled in section 2. The construction of such Chern numbers in (3) or (4) requires that band projectors satisfy appropriate continuity criteria. We observe from (21) that one point compactification is not applicable in this case. Even radial compactification and the definition of a BDI requires regularization effect that we will analyze in detail.

Although we treat k_z as a parameter, it is still a parameter of the excitation and not the underlying plasma or material model. Therefore we consider only phase transitions for constant k_z. In addition, we emphasize that only continuous variations in Ω, ω_p are considered here. Under these conditions, possible phase transitions and associated spectral gaps are identified as: transition from I$^\pm$ to II$^\pm$ for gaps $\ell = 1$ and $\ell = 2$; transition from II$^\pm$ to III$^\pm$ for gap $\ell = 1$; transition from I$^+$ to I$^-$ for gaps $\ell = 1$ and $\ell = 2$; transition from II$^+$ to II$^-$ for gaps $\ell = 1$ and $\ell = 2$; transition from IV$^+$ to IV$^-$ for gaps $\ell = 1$ and $\ell = 2$

for the 5×5 TM system. Comparison with Figure 2 verifies that all such transitions can be made by varying Ω, ω_p continuously with constant k_z. Additional continuous transitions with global spectral gaps are possible, but only as a superposition of the above transitions- e.g. for $\ell = 1$, a gapped III$^-$ to III$^+$ transition can be made continuously with k_z constant only as a superposition of transitions III$^- \to$ II$^- \to$ II$^+ \to$ III$^+$. Therefore analyzing the above transitions fully characterizes any continuous topological phase transitions when k_z is held constant.

Numerical diagonalization of the interface Hamiltonian H_I via finite differences is used to verify the BEC in each of the above cases. Of particular note is the fact that some branches of spectrum appear to be discontinuous. This is a product of our choice of periodic boundary conditions, which necessarily produce edge modes both at the transition of interest at $y = 0$ and at a spurious phase transition at the edge of our domain $y = L$ introduced by periodic boundary conditions. We choose to eliminate edge modes which appear at this spurious boundary for clarity but occasionally the same branch of spectrum will produce edge modes at $y = 0$ for $k_x > 0$ ($k_x < 0$) and at $y = L$ for $k_x < 0$ ($k_x > 0$), giving the appearance of a discontinuous branch of spectrum. Symmetry arguments and inclusion of spurious modes shows that these branches do not cross the band gap and thus do not contribute to σ_I, see Appendix E for details.

We now analyze these gaps and their topological properties, selecting $\pm$ above as being equal to $+$ for concreteness. The predicted number of edge states and the validity of the BEC (8) is illustrated in each case by numerical simulations of the spectral decomposition of the interface Hamiltonian.

BDI $\mathfrak{C}[\mathrm{I}_\ell^+, \mathrm{II}_\ell^+]$. Consider the transition from I$^+$ to II$^+$. Thanks to the reduced model (23) with $\tilde{\omega}_p = \gamma y$ with $\gamma > 0$ so that the Dirac operator is in phase I$^+$ for $y < 0$ and in phase II$^+$ for $y > 0$. In other words, $\omega_p^S < \omega_-(\Omega, k_z) < \omega_{L-}^S$ in phase I$^+$ while $\omega_{L-}^N < \omega_-(\Omega, k_z) < \omega_p^N$ in phase II$^+$.

We now wish to construct a BDI by radial compactification as one-point compactification cannot hold without regularizing the problem. Thanks to the invariance (14), it is sufficient to verify the gluing condition (5) at $\theta = 0$ for $\ell = 1$ (and we equivalently verify gluing for $\sum_{j \geq \ell} \Pi_j^h$). However, we observe that while $\Psi_{3,4}$ are the same in phases N and S, this is not the case for Ψ_2 in (21) since σ depends on ω_p and $\omega_p^N \neq \omega_p^S$ as a necessary condition to transition from I$^+$ to II$^+$ which sustains a global band gap.

For this reason, we assume that $\Omega = \Omega(k)$ and $\omega_p = \omega_p(k)$ in the definition (13). We observe that $\Psi_2^N = \Psi_2^S$ (up to a multiplicative phase in $U(1)$) provided that $\bar{\sigma} = \lim_{k \to \infty} |\Omega(k)|/\omega_p(k)$ exists (and is independent of the values of $(\Omega(0), \omega_p(0))$). In this case, we obtain from Table 1 a well-defined invariant for the gap $\ell = 1$ given by [33]

$$\mathfrak{C}[\mathrm{I}_1^+, \mathrm{II}_1^+] = (\frac{\bar{\sigma}}{\sqrt{1 + \bar{\sigma}^2}} + 1 - 1) - (\frac{\bar{\sigma}}{\sqrt{1 + \bar{\sigma}^2}} - 1 + 1 - 1) = 1. \qquad (26)$$

The above regularization generalizes the regularization models used in [33, 5], which consists in assuming that $\omega_p(k) \to 0$ as $k \to \infty$. The predicted number of edge modes is confirmed in the simulation shown in Figure 3.
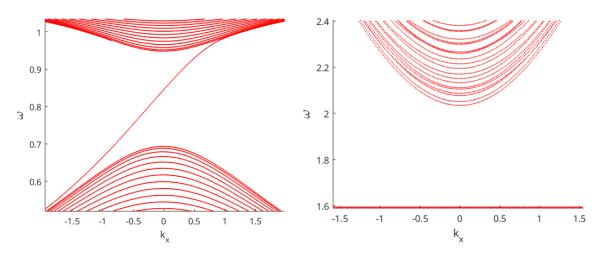
Figure 3: Numerically calculated spectrum with the parameters $(k_z, \Omega) = (2, 1)$ for the transition from phase I$^+$ to II$^+$ (ω_p varying from $0.5\omega_-$ to $1.5\omega_-$ with $\omega_- = 0.8284$ s^{-1}). Left shows the spectral gap between bands 1 and 2, which illustrates one topologically protected edge state, and right shows the spectral gap between bands 2 and 3, which has no edge states as predicted.

The above invariant is consistent with the BDI associated to the reduced Dirac operator in (23), where [14]

$$\mathfrak{C}[\mathfrak{D}^S, \mathfrak{D}^N] = 1.$$

We can similarly calculate that for $\ell = 2$:

$$\mathfrak{C}[\mathrm{I}_2^+, \mathrm{II}_2^+] = (1 - 1) - (-1 + 1) = 0, \tag{27}$$

which is also verified numerically in Figure 3. Since Ψ_3^N, Ψ_4^N are the same as Ψ_3^S, Ψ_4^S (5) holds without need for regularization in this case.

BDI $\mathfrak{C}[\mathrm{II}_\ell^+, \mathrm{III}_\ell^+]$. As we discussed in Section 3.5, there is no fully gapped transition from phase II$^+$ to III$^+$ for $\ell = 2$. However, the frequency branches 2 and 3 are still separated even if there is no global gap and the construction of a BDI is in fact independent of the presence of a global gap. Using the same regularization procedure as defined above, we would obtain a BDI equal to $\mathfrak{C}[\mathrm{II}^+, \mathrm{III}^+] = (0 - 1) - (1 - 1) = -1$ involving the gluing of $\Psi_{3,4}$, which is guaranteed without the need to regularize the problem.

A global band gap is possible for $\ell = 1$. Using the same regularization as in the previous paragraph, $\bar{\sigma} = \lim_{k \to \infty} |\Omega(k)|/\omega_p(k)$, the BDI is well-defined for this gap and we compute:

$$\mathfrak{C}[\mathrm{II}_1^+, \mathrm{III}_1^+] = (1 + \frac{\bar{\sigma}}{\sqrt{\bar{\sigma}^2 + 1}} - 1) - (\frac{\bar{\sigma}}{\sqrt{\bar{\sigma}^2 + 1}} + 1 - 1) = 0$$
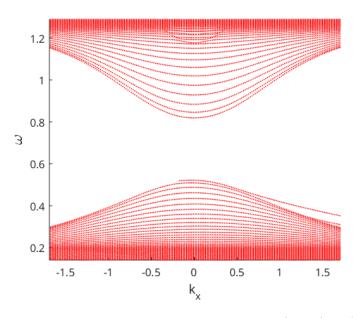
This result is verified numerically in Figure 4.

Figure 4: Numerically calculated spectrum with parameters $(k_z, \Omega) = (1, 1)$ for the transition from II$^+$ to III$^+$ (ω_p varying from $0.5\omega_+$ to $1.5\omega_+$ with $\omega_+ = 1.33$ s^{-1}).

BDI $\mathfrak{C}[\text{II}_\ell^-, \text{II}_\ell^+]$.   We now consider the transition for $\ell = 1$ between phases II$^+$ and II$^-$ assuming $\Omega^S < 0$ and $\Omega^N > 0$ in the construction of the interface Hamiltonian H_I. We observe that $\Gamma_P(0)\Gamma_\Omega = \text{Diag}(1, -1, 1, 1, -1, 1, 1, -1, 1)$ and we therefore need to glue together Ψ_2 and $\Gamma_P(0)\Gamma_\Omega\Psi_2$ in (21) (modulo a phase in $U(1)$) to define a BDI.

This is possible only when the term involving $\hat{e}_2$ vanishes as it transforms with a different sign from the other components. As a result, we need a regularization implying that $\bar{\sigma} = 0$ in the limit $k \to \infty$. We thus propose the regularization

$$\Omega(k) = (1 + \eta|k|^2)^{-\frac{1}{2}}\Omega(0), \tag{28}$$

with $\eta > 0$ arbitrarily small. This allows one to obtain

$$\mathfrak{C}[\text{II}_1^-, \text{II}_1^+] = (0 + 1 - 1) - (0 - 1 + 1) = 0. \tag{29}$$

This predicts the absence of topologically protected asymmetry separating phases II$^-$ and II$^+$, which we verify numerically in Figure 5.

In contrast, a regularization imposing $\omega_p(k) \to 0$ as $k \to \infty$, as in, e.g., [5, 33], leads to $\bar{\sigma} = \infty$ and a predicted an invariant equal to $(1 + 1 - 1) - (-1 - 1 + 1) = 2$. Note that the latter invariant, which is simply obtained by summing curvature integrals, is not a BDI since the projectors associated to Ψ_2^N and Ψ_2^S cannot be glued together continuously in a radial compactification. The numerical simulations in Figure 5 confirm that the predicted number of protected edge modes 2 is incorrect while $\mathfrak{C}[\text{II}_1^-, \text{II}_1^+] = 0$ is correct. Aside from the fact that (28) produces well-defined BDI's which agree with numerical results, we provide some physical justification for (28) in Appendix C as a high-wave number limit of a hydrodynamic model which allows for time-dependent perturbations in electron density.
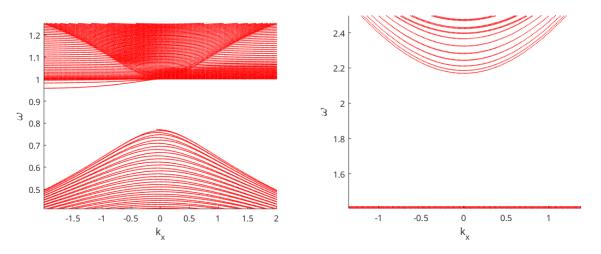
20

Figure 5: Numerically calculated spectrum with the parameters $(k_z, \omega_p) = (2, 1)$ for the transition from phase II$^-$ to II$^+$ with Ω varying from -0.75 to 0.75 s^{-1}. Left shows the spectral gap between bands 1 and 2 and right the gap between bands 2 and 3. No edge states are present as predicted by BDI's (29).

For $\ell = 2$ we again can rely on the fact that $\Psi_{3,4}$ are the same in phases N and S, so without regularization the BDI is well defined and:

$$\mathfrak{C}[\text{I}_2^+, \text{II}_2^+] = (1 - 1) - (-1 + 1) = 0. \tag{30}$$

Although it is clear that well defined BDI's predict 0 edge modes in this transition, a more heuristic argument can also be made for why this must be the case. Calculating the eigenvalues of (13) with $\Omega = 0$ is straightforward and produces positive eigenvalues $(\omega_1, \omega_2, \omega_3, \omega_4) = (0, \omega_p, \sqrt{\omega_p^2 + |\mathbf{k}|^2}, \sqrt{\omega_p^2 + |\mathbf{k}|^2})$. In phase II$^\pm$ we have that $k_z \neq 0 \Rightarrow |\mathbf{k}|^2 > 0$, therefore in the transition II$^- \rightarrow$ II$^+$ band 2 in fact does not cross any band. Hence band 2 cannot (at least in the continuous sense) exchange modes with another band, and all BDI's involving band 2 should intuitively be 0.

BDI $\mathfrak{C}[\text{IV}_\ell^-, \text{IV}_\ell^+]$. This corresponds to the case $k_z = 0$ and the analysis of the 5×5 system for TM modes. Focusing on TM modes, we observe the presence of two global gaps; a first one between $\tilde{\omega}_0 = 0$ and $\tilde{\omega}_1 = \omega_2$ and a second one between $\tilde{\omega}_1 = \omega_2$ and $\tilde{\omega}_2 = \omega_4$. The second gap is actually filled by TE modes corresponding to ω_3. We thus have a new gap not present in the 9×9 system, whose topological properties we now analyze.

As in the transition from II$^-$ to II$^+$, we assume the regularization (28). We thus obtain the two phase transitions (considering terms $\mathcal{C}_{2,4}$ in Table 1 while discarding $\mathcal{C}_{1,3}$, which are trivial anyway) corresponding to TE modes:

$$\mathfrak{C}[\text{IV}_1^-, \text{IV}_1^+] = (-1 + 1) - (1 - 1) = 0, \quad \mathfrak{C}[\text{IV}_2^-, \text{IV}_2^+] = (+1) - (-1) = 2. \tag{31}$$

One of the transitions is therefore topologically trivial while the second one predicts the presence of two edge modes. We see in the numerical simulations of Figure 6 that two edge

modes are indeed present in the gap $[\tilde{\omega}_1, \tilde{\omega}_2]$ while none are present in the gap $[0, \tilde{\omega}_1]$ for an interface Hamiltonian H_I where $\Omega(y)$ transitions from $-\Omega_0 < 0$ for H^S in phase IV$^-$ to $+\Omega_0 > 0$ for H^N in phase IV$^+$ (strictly speaking these absolute phases are not described by an invariant; only the phase difference is).
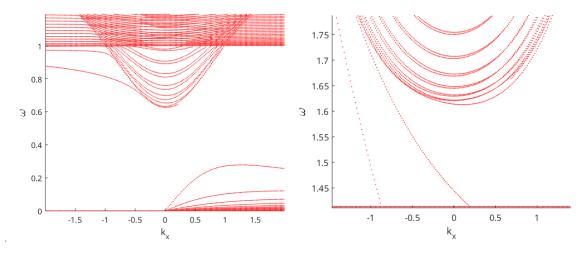

Figure 6: Numerically calculated spectrum with parameters $(k_z, \omega_p) = (0, 1)$ where Ω varies from -1 to 1 s^{-1}. Left shows the spectral gap between transverse magnetic modes 2 and 4, demonstrating 2 topologically protected edge modes as predicted. Right shows the gap between transverse magnetic modes 1 and 2, showing no edge modes, also consistent with prediction of BDI's.

Note that a regularization based on $\omega_p(k) \to 0$ as $k \to \infty$ (with $\sigma = \infty$ in Table 1) would predict phase transitions in these two spectral gaps given respectively by an incorrect $(-2+1) - (2-1) = -2$ and a correct $(1) - (-1) = 2$. We reiterate that these transitions, while described by integers, are not BDI as the gluing conditions (5) are not met.

It should be noted that many recent results [41, 42, 43, 44] have shown that here may be violations of the BEC in the transition $[\text{IV}_2^-, \text{IV}_2^+]$. Many of these arguments are based on physical limitations of the particular photonic/cold plasma model and non-local effects which are not considered here [42, 43, 44]. However, in [41] it was shown numerically and by Green's function analysis that only one topologically protected edge mode exists in the gapped transition $[\text{IV}_2^-, \text{IV}_2^+]$ although 2 were still predicted. While it would seem that our results differ, a key difference in our assumptions is the insistence of continuity of topological phase transitions, e.g. continuity of $\omega_p(y), \Omega(y)$. It was shown in [30] that in a 3×3 PDE model of shallow water equations which govern equatorial waves the BEC holds only when the parameters of the system are continuous. We expect that a similar result holds here and the effect of boundary regularity on BEC for photonic systems is the subject of future work. In addition, our analysis shows that these edge modes are not robust to perturbations in k_z around 0 so that even small deviations from $k_z = 0$ will couple topologically protected TM modes to bulk TE modes which fill the $\ell = 2$ TM spectral gap and allow dispersion into the bulk.

BDI $\mathfrak{C}[I^-, I^+]$. We note that the phases I^- and I^+ are not connected in the diagram in Figure 2 except throught the single point $(\Omega, \omega_p) = (0, 0)$. Still, we may envision a transition between these phases since they share a common gap for $\ell = 1$. We verify that eigenvectors may be glued together under the regularization assumption (28). We then obtain for the gap $\ell = 1$ the following invariant

$$\mathfrak{C}[I^-, I^+] = (1 - 1 + 1) - (-1 + 1 - 1) = 2. \tag{32}$$

We now show that such an invariant, even as it takes the form of a BDI, should not be trusted. To demonstrate this, we use the examples presented in section 2.5 and the reduced Dirac models introduced in (23) and (24). In both cases, we assume that $\tilde{\omega}_p < 0$. The transition from I^- to I^+ at the level of reduced models therefore corresponds to a transition from $\mathfrak{D}^S = \mathfrak{D}[-\Omega]$ to $\mathfrak{D}^N = \mathfrak{D}[\Omega]$.

This transition may be modeled as in section 2.5 by an anisotropic Fermi velocity $v_x(y)$ transitioning from $v_x(y) < 0$ for $y \leq -1$ to $v_x(y) > 0$ for $y \geq 1$. As we saw in section 2.5, this is a severe violation of ellipticity under which the BEC (8) is guaranteed to hold and as mentioned in that section, the BDI (32), even if guaranteed to be integer-valued, should not be trusted to provide information on the interface current observable and the number of edge modes. This is confirmed by numerical simulations in Figure 7, where transitions for the 9×9 system H_I from negative to positive values of Ω yield no discernible edge state, but rather displays a continuum of flat bands as predicted in section 2.5.
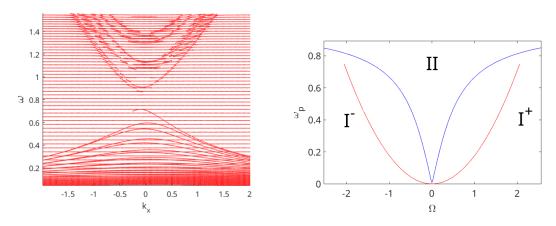

Figure 7: Numerically calculated spectrum for the I^- to I^+ transition. Right shows ω_p as a function of Ω for the transition considered plotted in red, which necessarily must pass through $(\omega_p, \Omega) = (0, 0)$ for such a transition to occur. Plotted in blue is ω_- as in Figure 1. Right is the numerically calculated spectrum using the profile on the right, showing a gap in bulk spectra, but the gap being filled by continuum modes as described in Section 2.5.

5 Conclusion

For a magnetically biased coupled light-matter Hamiltonian that finds applications in cold plasmas and macroscopic descriptions of photonic materials, we compute integrals of Berry

curvature for the eight possible topological phases the material can take. We identified common spectral gaps among topological phases, essentially recovering earlier work in [33, 21, 31, 8]. Without regularization, the integrals of Berry curvature are not integer-valued and do not represent stable topological invariants. A standard regularzation technique, introduced in [5], restores integer values to integrals of Berry curvature and allowed for the correct prediction of topologically protected edge states in two important cases [5, 35, 7].

Our main claim is that having integer-valued curvature integrals is not sufficient to predict the number of edge states at interfaces separating different bulk phases. Rather, regularization should aim to construct bulk difference invariants, which give a correct prediction of the bulk edge correspondence for elliptic operators. We constructed such BDI's using a novel regularization technique which has justification as the high-wave number limit of hydrodynamic considerations. Numerical spectral calculations verify that these BDI's predict the correct number of topologically protected edge states in all cases except one, in which the Hamiltonian is singular and cannot be expected to obey the BEC.

Acknowledgments

Appendices:

A   Invariants for continuous operators

We recall the definition of invariants for continuous operators following the review in [16]. Any continuous differential operator may be written as

$$H_I f(x) = (\mathrm{Op}^w \alpha) f(x) = \int_{\mathbb{R}^{2d}} \frac{e^{i(x-y)\cdot\xi}}{(2\pi)^d} \alpha(\frac{x+y}{2}, \xi) f(y) d\xi dy. \tag{33}$$

For the (possibly regularized) Dirac operator in dimension $d = 2$ with y-dependent coefficients, we have for instance

$$\alpha(y, \xi, \zeta) = v_x(y)\xi\sigma_1 + \zeta\sigma_2 + (m(y) + \eta(\xi^2 + \zeta^2))\sigma_3.$$

Associated to H_I is an operator

$$F = H_I - ix = \mathrm{Op}^w(\alpha - ix).$$

Under general conditions, F is a Fredholm operator, whose index $\mathrm{Index}F = \mathrm{dimKer}F - \mathrm{dimKer}F^*$ is given by the formula

$$\mathrm{Index}F = \mathrm{F}_2[a] := \frac{1}{24\pi^2} \int_{\mathbb{S}_R^4} \mathrm{tr}(a^{-1}da)^{\wedge 3}, \tag{34}$$

where $\mathbb{S}_R^4$ is the 4-sphere in phase space of radius R. Here, R is chosen large enough that a^{-1} is defined on it. For the Dirac operator, where the singularities occur at $(x, y, \xi, \zeta) = 0$,

any $R > 0$ would do. This integral may be estimated in various ways [16, 14] and gives the result $\mathrm{F}_2[a] = -\operatorname{sign}(v_x)$ for $m(y) = y$ or $m(y) = \operatorname{sign}(y)$ for instance and $v_x \neq 0$ constant. For $v_x(y) = \arctan y$ and $\eta > 0$, then we find $\mathrm{F}_2[a] = -2$.

Under general hypotheses satisfied by Dirac operators and more generally elliptic operators, we have that

$$\mathrm{F}_2[a] := \int_{\mathcal{C}_L} \operatorname{tr}(a^{-1}da)^{\wedge 3},$$

where $\mathcal{C}_L = \{y = L\} \cup \{y = -L\}$. This implies that $\mathrm{F}_2[a]$ is a BDI since it depends on the coefficients of $H_I = \mathrm{Op}^w \alpha$ only at $y = \pm R$ in the N and S hemispheres. Moreover, some calculations [2, 16] show that

$$\mathrm{F}_2[a] = \mathrm{BDI} = \mathfrak{C}[\Pi^S, \Pi^N].$$

For elliptic operators, we further obtain that the BEC (8) holds. In this context, ellipticity means that $\alpha(y, \xi, \zeta)$ has singular values that grow at least linearly as $(\xi, \zeta) \to \infty$. Other ellipticity conditions are proposed in [13, 14, 16]. We note that the absence of regularization, i.e. for $\eta = 0$, the operator H_I is not elliptic when $v_x(y)$ is allowed to vanish for at such points the singular values of α do not grow linearly as $\xi \to \infty$. .

B Relation to dielectric tensor in photonics

Let $\psi = (E, B)^T$ and recast the spectral problem for the cold plasma Hamiltonian as

$$\begin{pmatrix} A & B \\ B^* & C \end{pmatrix} \begin{pmatrix} v \\ \psi \end{pmatrix} = \omega \begin{pmatrix} v \\ \psi \end{pmatrix}.$$

Elimination of v assuming ω not in the spectrum of A yields by Schur complement the relation $(C - B^*(A - \omega)B)\psi = \omega\psi$ or equivalently

$$C\psi = \omega M(\omega)\psi, \qquad M(\omega) := I - \frac{1}{\omega} B^*(\omega - A)^{-1} B.$$

For the Hamiltonian in (13), we find

$$M = \operatorname{Diag}(\bar{\epsilon}, I_3), \qquad \bar{\epsilon} = \begin{pmatrix} \epsilon_1 & \epsilon_{12} & 0 \\ -\epsilon_{12} & \epsilon_1 & 0 \\ 0 & 0 & \epsilon_3 \end{pmatrix}$$

where the coefficients in the plasma dielectric tensor ϵ are given as in [33, 5, 31] by $\epsilon_1 = 1 - \frac{\omega_p^2}{\omega^2 - \Omega^2}$, $\epsilon_3 = 1 - \frac{\omega_p^2}{\omega^2}$, and the non-reciprocal component $\epsilon_{12} = i \frac{-\Omega \omega_p^2}{\omega(\omega^2 - \Omega^2)}$.

The analysis of topological phases presented in the paper presumably extends to more general models of photonic materials [5, 31, 45] and this will be explored in future work.

Let us conclude this section with a comment on the computation of Berry connections $\mathcal{A}$ in the context of the above elimination of the component v. Let us assume that A and

B are independent of $\mathbf{k}$, which holds in the absence of regularization. The connection of the full field $(v, \psi)^T$ is defined for the above model as:

$$v \cdot dv + \psi \cdot d\psi = (B^*(\omega - A)^{-2} B + I)\psi \cdot d\psi = \psi \cdot \partial_\omega (\omega - B^*(\omega - A)^{-1} B) d\psi.$$

Note that the normalization of eigenvectors is

$$v \cdot v + \psi \cdot \psi = (B^*(\omega - A)^{-2} B + I)\psi \cdot \psi = \psi \cdot \partial_\omega (\omega - B^*(\omega - A)^{-1} B)\psi.$$

Thus,

$$v \cdot dv + \psi \cdot d\psi = \frac{v \cdot dv + \psi \cdot d\psi}{v \cdot v + \psi \cdot \psi} = \frac{\psi \cdot \partial_\omega (\omega M(\omega)) d\psi}{\psi \cdot \partial_\omega (\omega M(\omega))\psi},$$

which is the formula for the computation of Berry connections and Berry curvatures considered in [3, 5] as the natural expression of Berry connections after elimination of the component v. We note that the above formula applies more generally for $M = M(\mathbf{k}, \omega)$ [3, 5].

C Regularization

This section provides some possible heuristic justification for the regularization proposed in (28). We recast the electron transport equation for current $\tilde{v}$ as

$$\partial_t \tilde{v} = \Omega e_z \times \tilde{v} - \omega_p \tilde{E}.$$

Let us now assume as in [32, 34] the presence of a density term ρ satisfying the continuity equation $\partial_t \rho + \nabla \cdot \tilde{v} = 0$ and modifying the above transport equation to include collisions as

$$\partial_t \tilde{v} + \beta^2 \nabla \rho = \Omega e_z \times \tilde{v} - \omega_p \tilde{E}.$$

These equations in dual variables are given by (with the convention $i\partial_t \equiv \omega$)

$$\omega \tilde{v} - \beta^2 \mathbf{k} \rho = i\Omega e_z \times \tilde{v} - i\omega_p \tilde{E}, \qquad -\omega \rho + \mathbf{k} \cdot \tilde{v} = 0.$$

Eliminating ρ gives

$$\omega (1 - \frac{\beta^2 \mathbf{k} \otimes \mathbf{k}}{\omega^2})\tilde{v} = i\Omega e_z \times \tilde{v} - i\omega_p \tilde{E}.$$

Define

$$v = (1 + \frac{\beta^2}{\omega^2} \mathbf{k} \otimes \mathbf{k})^{\frac{1}{2}} \tilde{v}, \quad E = (1 + \frac{\beta^2}{\omega^2} \mathbf{k} \otimes \mathbf{k})^{-\frac{1}{2}} \tilde{E}$$

to obtain

$$(1 - \frac{\beta^2 \mathbf{k} \otimes \mathbf{k}}{\omega^2})(1 + \frac{\beta^2 \mathbf{k} \otimes \mathbf{k}}{\omega^2})^{-1} \omega v = i\Omega (1 + \frac{\beta^2}{\omega^2} \mathbf{k} \otimes \mathbf{k})^{-\frac{1}{2}} e_z \times (1 + \frac{\beta^2}{\omega^2} \mathbf{k} \otimes \mathbf{k})^{-\frac{1}{2}} v - i\omega_p E.$$

Denoting by $\Pi = \hat{\mathbf{k}} \otimes \hat{\mathbf{k}}$ the projector onto the direction $\hat{\mathbf{k}} = \mathbf{k}/k$, we observe that the term on the left-hand side is

$$\left(I - \Pi + \frac{1 - \frac{\beta^2 k^2}{\omega^2}}{1 + \frac{\beta^2 k^2}{\omega^2}} \Pi \right) \omega v.$$

For $|\boldsymbol{k}|$ large, we further obtain after some algebra that:

$$(1 + \frac{\beta^2}{\omega^2}\boldsymbol{k} \otimes \boldsymbol{k})^{-\frac{1}{2}}\Omega e_z \times (1 + \frac{\beta^2}{\omega^2}\boldsymbol{k} \otimes \boldsymbol{k})^{-\frac{1}{2}} \approx (1 + \frac{\beta^2 k^2}{\omega^2})^{-\frac{1}{2}}\Omega e_z \times .$$

Therefore, in that limit

$$\omega(I - 2\Pi)v \approx (1 + \frac{\beta^2 k^2}{\omega^2})^{-\frac{1}{2}}\Omega e_z \times -i\omega_p E.$$

We observe that the component of $\Psi_{1,2}$ in (21) that needs regularization is v_2, i.e., the component orthogonal to $\boldsymbol{k} = (k_x, 0, k_z)$. This is therefore a component in the kernel of $\boldsymbol{k} \otimes \boldsymbol{k}$ for which the above with $\Pi v = 0$ applies. This provides some heuristics for the regularization introduced in (28) for any band where ω does not converge to 0 as $k \to \infty$, which is the case for the bands we are interested in. We stress again that the numerical simulations performed in section 4 were obtained without any regularization of the Hamiltonian. We do not have a complete justification of (8) for either regularized or un-regularized Hamiltonians.

D   Reduced two-band models

This section provides additional information on the derivation of (24) and (23) when $\Omega \to -\Omega$. The degenerate eigenvectors associated to $\omega_p = \omega_-$ when $\mathbf{k} = 0, k_z, \Omega > 0$, denoted ψ_{10}, ψ_{20} are:

$$\psi_{10} = \frac{1}{\sqrt{2}}(\hat{e}_z, i\hat{e}_z, 0)^T, \quad \psi_{20} = c\left(i\frac{k_z^2}{|\Omega|}\hat{e}_+, \omega_-\hat{e}_+, -ik_z\hat{e}_+\right)^T$$

for an appropriate normalizing constant c. To obtain a 2x2 approximation of $H(\mathbf{k})$ around the point $\mathbf{k} = 0, \omega_p = \omega_-$ we then project $H(\mathbf{k})$ onto ψ_{10}, ψ_{20}. Since the model is an approximation around $\mathbf{k} = 0$ and $\omega_p = \omega_-$ we split H into:

$$H(\mathbf{k}) = H_0 + \tilde{H}(\mathbf{k}) = \begin{pmatrix} i\Omega\hat{e}_z\times & -i\omega_- & 0 \\ i\omega_- & 0 & -k_z\hat{e}_z\times \\ 0 & k_z\hat{e}_z\times & 0 \end{pmatrix} + \begin{pmatrix} 0 & -i\tilde{\omega} & 0 \\ i\tilde{\omega} & 0 & -\mathbf{k}\times \\ 0 & \mathbf{k}\times & 0 \end{pmatrix}.$$

When $\tilde{\omega}$ is a small positive value the $H(\mathbf{k})$ is in phase II$^+$ and when $\tilde{\omega}$ is small an negative $H(\mathbf{k})$ is in phase I$^+$. Clearly ψ_{10}, ψ_{20} are eigenvectors of H_0 both with eigenvalue ω_-. With $\hat{z} \times e_+ = -ie_+$ we find

$$\tilde{H}(\mathbf{k})\psi_{20} = c\begin{pmatrix} -i\tilde{\omega}\omega_-\hat{e}_+ \\ (-\frac{k_z^2}{|\Omega|}\tilde{\omega} + ik_z\mathbf{k}\times)\hat{e}_+ \\ \omega_-\mathbf{k}\times\hat{e}_+ \end{pmatrix} \quad \mathbf{k}\times\hat{e}_+ = \frac{1}{\sqrt{2}}\begin{pmatrix} 0 \\ 0 \\ ik_x - k_y \end{pmatrix} \quad \mathbf{k}\times\hat{e}_- = \frac{1}{\sqrt{2}}\begin{pmatrix} 0 \\ 0 \\ -ik_x - k_y \end{pmatrix},$$

from which we deduce, since $(\hat{e}_z, \hat{e}_\pm) = 0$:

$$(\psi_{10}, \tilde{H}(\mathbf{k})\psi_{20}) = \frac{ck_z}{\sqrt{2}}(ik_x - k_y), \quad (\psi_{20}, \tilde{H}(\mathbf{k})\psi_{10}) = -\frac{k_z c}{\sqrt{2}}(ik_x + k_y),$$

27

$$(\psi_{10}, \tilde{H}(\mathbf{k})\psi_{10}) = \tilde{\omega}, \quad (\psi_{20}, \tilde{H}(\mathbf{k})\psi_{20}) = \frac{-2\omega_- c^2 k_z^2}{|\Omega|}\tilde{\omega}.$$

After explicit calculation of c this yields (23). Now note that $S(\theta)\hat{e}_z = \hat{e}_z$ so that $\tilde{\Gamma}_P(\theta)\psi_{10} = \psi_{10}$, but $S(\theta)\hat{e}_+ = e^{i2\theta}\hat{e}_-$ implying that

$$\tilde{\Gamma}_P(\theta)\psi_{20} = e^{i2\theta}(i\frac{k_z^2}{|\Omega|}\hat{e}_-, \omega_-\hat{e}_-, ik_z\hat{e}_-)^T.$$

This phase will necessarily cancel out in the diagonal elements $(\psi_{20}, \tilde{H}(\mathbf{k})\psi_{20})$ and $(\psi_{10}, \tilde{H}(\mathbf{k})\psi_{10})$ but for the off-diagonal terms we obtain:

$$(\psi_{10}, H(\mathbf{k})\tilde{\Gamma}_P(\theta)\psi_{20}) = e^{i2\theta}\frac{k_z c}{\sqrt{2}}(ik_x + k_y), \quad (\psi_{20}, H(\mathbf{k})\tilde{\Gamma}_P(\theta)\psi_{10}) = e^{i2\theta}\frac{ck_z}{\sqrt{2}}(k_y - ik_x).$$

Again with explicit calculation of c we obtain (24). θ is arbitrary since $\mathbf{k} = 0$ for ψ_{10}, ψ_{20}. Therefore this shows that the transition from Ω to $-\Omega$ yields $(k_x, k_y) \to (k_x, -k_y)$ for $\theta = 0$ while $(k_x, k_y) \to (-k_x, k_y)$ for $\theta = \frac{\pi}{2}$ for instance. This arbitrary phase could have also been deduced from adding an arbitrary phase to ψ_{10} or ψ_{20} and reflects the rotational invariance of the problem. This justifies the form of the models deduced in section 3.5.

E   Numerical simulations

We follow a similar finite difference scheme as [7][30] to numerically calculate the spectrum of the interface Hamiltonian H_I. We choose to vary the parameters ω_p, Ω in the y-direction so that the Hamiltonian is invariant with respect to translations in x. Taking the Fourier transform of (12) in t, x, z gives:

$$\omega\psi(y) = \begin{pmatrix} i\Omega(y)\hat{e}_z\times & -i\omega_p(y) & 0 \\ i\omega_p(y) & 0 & i\partial_y\hat{e}_y \times -(k_x, 0, k_z)^t\times \\ 0 & -i\partial_y\hat{e}_y \times +(k_x, 0, k_z)^t\times & 0 \end{pmatrix}\psi(y)$$

which is an ODE in y for each k_x. Discretizing y into N points on an interval $[-L, L]$ allows us to approximate the equation as:

$$\omega\psi(y_i) = H_i^- \psi(y_{i-1}) + H_i\psi(y_i) + H_i^+\psi(y_{i+1}) \tag{35}$$

$$H_i = \begin{pmatrix} i\Omega(y_i)\hat{e}_z\times & -i\omega_p(y_i) & 0 \\ i\omega_p(y_i) & 0 & \frac{i}{\Delta y}\hat{e}_y \times -\frac{1}{2}(k_x, 0, k_z)^t\times \\ 0 & -\frac{i}{\Delta y}\hat{e}_y \times +\frac{1}{2}(k_x, 0, k_z)^t\times & 0 \end{pmatrix}$$

$$H_i^- = \begin{pmatrix} 0 & 0 & 0 \\ 0 & 0 & -D \\ 0 & 0 & 0 \end{pmatrix} \quad H_i^+ = \begin{pmatrix} 0 & 0 & 0 \\ 0 & 0 & 0 \\ 0 & D & 0 \end{pmatrix} \quad D = \frac{i}{\Delta y}\hat{e}_y \times +\frac{1}{2}(k_x, 0, k_z)^t\times$$

where $\Delta y = 2L/N$. We adopt the particular combination of forward and backward differences and averaging E, B in the second and third row from [7] to ensure the discrete problem obeys the same particle-hole symmetry as the continuous one. This convention amounts to discretizing B on half-integer grid points. Calculating the eigenvalues of H_I can then be done by diagonalizing a $9N \times 9N$ matrix. In order to ensure the matrix is Hermitian periodic boundary conditions are enforced $(\psi(-L) = \psi(L), \omega_p(-L) = \omega_p(L), \Omega(-L) = \Omega(L))$. Assuming our parameters cross from one topological phase into another, having periodic parameters Ω, ω_p introduces a second topological transition in the opposite direction, which will necessarily produce edge states concentrated around this second edge (in cases where edge states exist). For clarity, we adopt the strategy used in [30] and eliminate eigenvalues whose associated eigenvector has more than half its weight within $0.1L$ of the spurious edge.
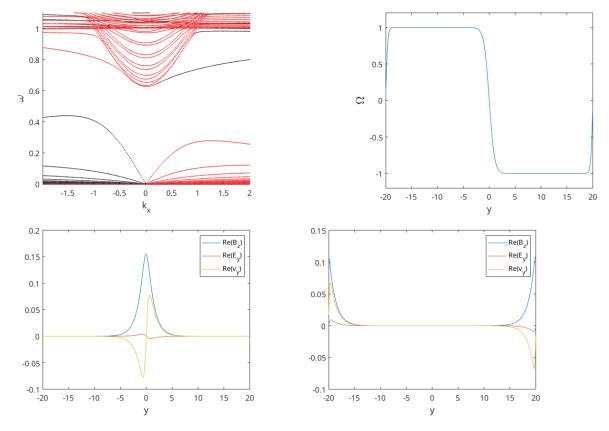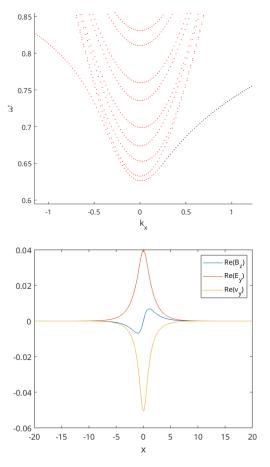

Figure 8: Illustration of the elimination of spurious edge modes for the spectrum calculated in Figure 6. Upper left shows the spectrum with spurious modes shown in black. Upper right is the profile of Ω, which consists of a periodic combination of logistic functions. The bottom row shows components of the numerically calculated eigenvectors plotted as a function of y. Left is an edge mode, specifically the eigenvector associated to $(k_x, \omega) = (0.5, 0.1919)$, while right is a mode concentrated around the spurious edge $((k_x, \omega) = (-0.5, 0.2636))$. Modes of the latter type are eliminated for clarity as discussed above.

One disadvantage of this method is the appearance of continuous branches of spectrum which are edge modes concentrated at $y = 0$ for $k_x < 0$ ($k_x > 0$) and concentrated at $y = L$ for $k_x > 0$ ($k_x < 0$). Figure 8 illustrates one such branch. Since we have two topological phase
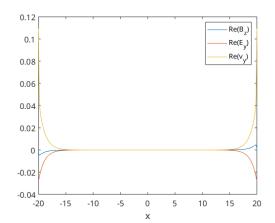
Figure 9: Illustration of branches described in the last paragraph of Appendix E which exhibit both spurious and edge modes. Upper left is an inset of the spectrum showed in Figure 8 showing the bottom-most branch transitioning continuously from a spurious mode to a valid one. Upper right shows the eigenvector associated to this branch at $k_x = 1$ and bottom the eigenvectors associated to this branch at $k_x = -1$.

transitions in opposite directions, we expect that each uni-directional edge state localized at $y = 0$ for $k_{x0} < 0$ will be mirrored by a uni-directional edge state localized at $y = L$ for $k_{xL} = -k_{x0}$. For bands which cross a spectral gap (topologically protected edge states) this produces a mirrored band localized at $y = L$ which produces an identical spectral flow in the opposite direction (see [7, 33]). However for edge states whose energy does not overlap with the spectral gap, bands may appear to switch from concentrated at $y = 0$ for $k_x < 0$ ($k_x > 0$) to concentrated at $y = L$ for $k_x > 0$ ($k_x < 0$) as we see in Figure 9. The appearance of these bands is therefore due to the periodic boundary conditions we impose and we expect that such bands would not appear when considering more realistic boundary conditions. Inclusion of the spurious modes shows as in Figures 8 and 9 shows that these branches indeed only exist at energies outside the spectral gap and therefore do not contribute to σ_I.

F Topological Phase and Explicit Eigenvector Calculations

First we prove the inequality $\omega_{L-} < \omega_R < \omega_{L+}$. This can be proved from (19), copied here for in a more convenient form for this derivation:

$$k_z^2 = \omega_R^2 - \frac{\omega_p^2}{1 + \frac{\Omega}{\omega_R}}, \qquad k_z^2 = \omega_L^2 - \frac{\omega_p^2}{1 - \frac{\Omega}{\omega_L}}.$$

Notice from (19) that as $k_z \to \infty$, ω_L has two positive solutions, $\omega_L \to \Omega$ from below, and $\omega_L \to \sqrt{k_z^2 + \omega_p^2} \to \infty$. By continuity of eigenvalues then we know that there are two positive branches of ω_L, one of which is $0 < \omega_{L-} < \Omega$ and one of which is $\Omega < \omega_{L+}$ since $k_z^2 \to \pm\infty$ if ω_L approaches Ω, which would violate continuity of $\omega_{L\pm}$ as a function of k_z. Also notice that for $\Omega > 0$ and $\omega_R > 0$:

$$0 < \frac{\omega_p^2}{1 + \frac{\Omega}{\omega_R}} < \omega_p^2 \quad \Rightarrow \quad k_z^2 < \omega_R^2 < \omega_p^2 + k_z^2.$$

Next since we know that $\omega_{L+} > \Omega$ so that we also have $0 < \Omega/\omega_{L+} < 1$ so that:

$$\omega_{L+}^2 = k_z^2 + \frac{\omega_p^2}{1 - \frac{\Omega}{\omega_{L+}}} > k_z^2 + \omega_p^2$$

so indeed $\omega_{L+} > \omega_R$ and in addition $\omega_{L+} > \omega_p$. Finally since $\omega_{L-} < \Omega \Rightarrow \Omega/\omega_{L-} > 1$:

$$\omega_{L-}^2 - k_z^2 = \frac{\omega_p^2}{1 - \frac{\Omega}{\omega_{L-}}} < 0 \quad \Rightarrow \quad \omega_{L-}^2 < k_z^2.$$

To summarize we have proved that:

$$\omega_{L-}^2 < \min\{\Omega^2, k_z^2\} \leq k_z^2 < \omega_R < k_z^2 + \omega_p^2 < \omega_{L+},$$

so indeed $\omega_{L-} < \omega_R < \omega_{L+}$. This proves that when $k = 0$ the only band crossings occur at $\omega_p = \omega_\pm$. Again we rely on extensive numerical evidence that band crossings do not occur except when $k = 0$, $k_z = 0$, or $\Omega = 0$. Therefore the topological phases are completely determined by the curves $k_z = 0$, $\Omega = 0$, and $\omega_p = \omega_\pm$, which divide the parameter space into phases $I^\pm, II^\pm, III^\pm, IV^\pm$ as shown in Figure 1.

We also wish to point out more explicit forms of (21), (16), (17) which make the gluing conditions more explicit. (21) represents the eigenvectors as $k \to \infty$ for $\mathbf{k} = k\hat{e}_x$. Using (14) we can obtain eigenvectors for arbitrary $\mathbf{k}$ by applying R(θ) to Ψ_n, which amounts to applying $R(\theta)$ to each of v, E, B components of Ψ_n. Denote the unit $\mathbf{k}$ direction $\hat{\mathbf{k}} = \mathbf{k}/|\mathbf{k}|$. Noting that $R(\theta)$ leaves the $\hat{e}_z$ component invariant and $\hat{e}_y = \hat{e}_z \times \hat{e}_x = \hat{e}_z \times \hat{\mathbf{k}}(\theta = 0)$ we get:

$$\Psi_1(\mathbf{k}, \Omega) = \begin{pmatrix} -\frac{1}{\sqrt{1+\sigma^2}} R(\theta)(\hat{e}_z \times \hat{\mathbf{k}}(\theta = 0)) + i\hat{e}_z \\ -\frac{\sigma}{\sqrt{1+\sigma^2}} R(\theta)\hat{\mathbf{k}}(\theta = 0) \\ 0 \end{pmatrix} = \begin{pmatrix} \frac{1}{\sqrt{1+\sigma^2}}\hat{\mathbf{k}} \times \hat{e}_z + i\hat{e}_z \\ -\frac{\sigma}{\sqrt{1+\sigma^2}}\hat{\mathbf{k}} \\ 0 \end{pmatrix}.$$

Similarly for the remaining eigenvectors as $k \to \infty$:

$$\Psi_2(\mathbf{k}, \Omega) = \begin{pmatrix} \frac{\sigma}{\sqrt{1+\sigma^2}}\hat{\mathbf{k}} \times \hat{e}_z - i\hat{e}_z \\ \frac{1}{\sqrt{1+\sigma^2}}\hat{\mathbf{k}} \\ 0 \end{pmatrix} \qquad \Psi_3(\mathbf{k}, \Omega) = \begin{pmatrix} 0 \\ \hat{e}_z \\ \hat{\mathbf{k}} \times \hat{e}_z \end{pmatrix} \qquad \Psi_4(\mathbf{k}, \Omega) = \begin{pmatrix} 0 \\ -\hat{\mathbf{k}} \times \hat{e}_z \\ \hat{e}_z \end{pmatrix}$$

where these expressions are valid assuming $\Omega > 0$.

As mentioned in Section 3.2 the Hamiltonian also obeys parity symmetry under the anti-unitary operator $\Gamma_k K$, where K is the operator performing element-wise complex conjugation such that $\Gamma_k K H(\theta) K \Gamma_k = -H(\theta)$. To be more explicit we have $H(\mathbf{k})(\Gamma_k K \Psi_n(\mathbf{k})) = -\omega_n(\Gamma_k K \Psi_n(\mathbf{k})) = \omega_{-n}(\Gamma_k K \Psi_n(\mathbf{k}))$. Therefore the corresponding eigenvectors for $\omega \to -\omega$ are:

$$\Psi_{-1}(\mathbf{k}, \Omega) = \begin{pmatrix} \frac{1}{\sqrt{1+\sigma^2}}\hat{\mathbf{k}} \times \hat{e}_z - i\hat{e}_z \\ -\frac{\sigma}{\sqrt{1+\sigma^2}}\hat{\mathbf{k}} \\ 0 \end{pmatrix} \qquad \Psi_{-2}(\mathbf{k}, \Omega) = \begin{pmatrix} \frac{\sigma}{\sqrt{1+\sigma^2}}\hat{\mathbf{k}} \times \hat{e}_z + i\hat{e}_z \\ \frac{1}{\sqrt{1+\sigma^2}}\hat{\mathbf{k}} \\ 0 \end{pmatrix}$$

$$\Psi_{-3}(\mathbf{k}, \Omega) = \begin{pmatrix} 0 \\ \hat{e}_z \\ -\hat{\mathbf{k}} \times \hat{e}_z \end{pmatrix} \qquad \Psi_{-4}(\mathbf{k}, \Omega) = \begin{pmatrix} 0 \\ -\hat{\mathbf{k}} \times \hat{e}_z \\ -\hat{e}_z \end{pmatrix}.$$

Then by combining with Γ_Ω from Section 3.2 ($\Gamma_\Omega H(\mathbf{k}, \Omega)\Gamma_\Omega = -H(\mathbf{k}, -\Omega)$), we get $H(\mathbf{k}, -\Omega) = \Gamma_k K \Gamma_\Omega H(\mathbf{k}, \Omega)\Gamma_\Omega K \Gamma_k$ and subsequently:

$$\Psi_1(\mathbf{k}, -\Omega) = \begin{pmatrix} \frac{1}{\sqrt{1+\sigma^2}}\hat{\mathbf{k}} \times \hat{e}_z - i\hat{e}_z \\ \frac{\sigma}{\sqrt{1+\sigma^2}}\hat{\mathbf{k}} \\ 0 \end{pmatrix} \qquad \Psi_2(\mathbf{k}, -\Omega) = \begin{pmatrix} \frac{\sigma}{\sqrt{1+\sigma^2}}\hat{\mathbf{k}} \times \hat{e}_z + i\hat{e}_z \\ -\frac{1}{\sqrt{1+\sigma^2}}\hat{\mathbf{k}} \\ 0 \end{pmatrix}$$

$$\Psi_3(\mathbf{k}, -\Omega) = \begin{pmatrix} 0 \\ -\hat{e}_z \\ -\hat{\mathbf{k}} \times \hat{e}_z \end{pmatrix} \qquad \Psi_4(\mathbf{k}, -\Omega) = \begin{pmatrix} 0 \\ \hat{\mathbf{k}} \times \hat{e}_z \\ -\hat{e}_z \end{pmatrix}$$

$$\Psi_{-1}(\mathbf{k}, -\Omega) = \begin{pmatrix} \frac{1}{\sqrt{1+\sigma^2}}\hat{\mathbf{k}} \times \hat{e}_z + i\hat{e}_z \\ \frac{\sigma}{\sqrt{1+\sigma^2}}\hat{\mathbf{k}} \\ 0 \end{pmatrix} \qquad \Psi_{-2}(\mathbf{k}, -\Omega) = \begin{pmatrix} \frac{\sigma}{\sqrt{1+\sigma^2}}\hat{\mathbf{k}} \times \hat{e}_z - i\hat{e}_z \\ -\frac{1}{\sqrt{1+\sigma^2}}\hat{\mathbf{k}} \\ 0 \end{pmatrix}$$

$$\Psi_{-3}(\mathbf{k}, -\Omega) = \begin{pmatrix} 0 \\ -\hat{e}_z \\ \hat{\mathbf{k}} \times \hat{e}_z \end{pmatrix} \qquad \Psi_{-4}(\mathbf{k}, -\Omega) = \begin{pmatrix} 0 \\ \hat{\mathbf{k}} \times \hat{e}_z \\ \hat{e}_z \end{pmatrix}.$$

This is an exhaustive list of limiting eigenvectors as $k \to \infty$ in any case except the singular cases $k_z = 0$ and $\Omega = 0$. It is clear that as long as $\sigma(k) \to \bar{\sigma}$ independent of topological phase that Π_n^N glues to Π_n^S as long as Ω has the same sign for both N and S. However as soon as Ω changes sign this is not the case. There are two regularizations which produce integers for $\mathcal{C}[P_\ell^h]$ and hence integers for $\mathfrak{C}[P_\ell^S, P_\ell^N]$ when Ω changes sign, namely $\omega_p(k) \to 0$ and $\Omega \to 0$ respectively as $k \to \infty$, which correspond to $\sigma \to \infty$ and $\sigma \to 0$ respectively. Comparing eigenvectors in these two limits we see that in the $\omega_p(k) \to 0$ case:

$$\Pi_j(\mathbf{k}, -\Omega) = \Pi_j(\mathbf{k}, \Omega), \ j \in \{1, 3, 4\}; \quad \Pi_2(\mathbf{k}, -\Omega) = \Pi_{-2}(\mathbf{k}, \Omega).$$

So while (5) holds for $P_\ell^{N/S}$ when $\ell = 2$ regardless of a change of sign in Ω, it does not hold for $\ell = 1$. Meanwhile for $\Omega \to \infty$ we get:

$$\Pi_1(\mathbf{k}, -\Omega) = \Pi_{-1}(\mathbf{k}, \Omega); \quad \Pi_j(\mathbf{k}, -\Omega) = \Pi_j(\mathbf{k}, \Omega), \ \ j \in \{2, 3, 4\},$$

so (5) holds for $\ell = 1, 2$ regardless of a change of sign of Ω.

References

[1] M Zahid Hasan and Charles L Kane. Colloquium: topological insulators. *Reviews of modern physics*, 82(4):3045–3067, 2010.

[2] B Andrei Bernevig and Taylor L Hughes. *Topological insulators and topological superconductors*. Princeton university press, 2013.

[3] F. D. M. Haldane and S. Raghu. Possible realization of directional optical waveguides in photonic crystals with broken time-reversal symmetry. *Phys. Rev. Lett.*, 100:013904, Jan 2008.

[4] Ling Lu, John D Joannopoulos, and Marin Soljačić. Topological photonics. *Nature Photonics*, 8(11):821–829, 2014.

[5] Mário G Silveirinha. Chern invariants for continuous media. *Physical Review B*, 92(12):125153, 2015.

[6] Pierre Delplace, JB Marston, and Antoine Venaille. Topological origin of equatorial waves. *Science*, 358(6366):1075–1077, 2017.

[7] Yichen Fu and Hong Qin. Topological phases and bulk-edge correspondence of magnetized cold plasmas. *Nature Communications*, 12(1):3924, 2021.

[8] Jeffrey B Parker, JB Marston, Steven M Tobias, and Ziyan Zhu. Topological gaseous plasmon polariton in realistic plasma. *Physical Review Letters*, 124(19):195001, 2020.

[9] Joseph E. Avron, Ruedi Seiler, and Barry Simon. Quantum Hall effect and the relative index for projections. *Phys. Rev. Lett.*, 65:2185–2188, Oct 1990.

[10] Shun-Qing Shen. *Topological insulators*, volume 174. Springer, 2012.

[11] Guillaume Bal. Continuous bulk and interface description of topological insulators. *Journal of Mathematical Physics*, 60(8), 2019.

[12] Emil Prodan and Hermann Schulz-Baldes. *Bulk and boundary invariants for complex topological insulators: From K-Theory to Physics*. Springer Verlag, Berlin, 2016.

[13] Guillaume Bal. Topological invariants for interface modes. *Communications in Partial Differential Equations*, 47(8):1636–1679, 2022.

[14] Solomon Quinn and Guillaume Bal. Approximations of interface topological invariants. *SIAM Journal on Mathematical Analysis*, 56(4):5521–5582, 2024.

[15] Sylvain Rossi and Alessandro Tarantola. Topology of 2D Dirac operators with variable mass and an application to shallow-water waves. *Journal of Physics A: Mathematical and Theoretical*, 57(6):065201, 2024.

[16] Guillaume Bal. Continuous topological insulator, classification and bulk edge correspondence. *arXiv preprint arXiv:2412.00919*, 2024.

[17] Guillaume Bal, Paul Cazeaux, Daniel Massatt, and Solomon Quinn. Mathematical models of topologically protected transport in twisted bilayer graphene. *Multiscale Modeling & Simulation*, 21(3):1081–1121, 2023.

[18] Guillaume Bal and Daniel Massatt. Multiscale invariants of Floquet topological insulators. *Multiscale Modeling & Simulation*, 20(1):493–523, 2022.

[19] Yasuhiro Hatsugai. Chern number and edge states in the integer quantum Hall effect. *Physical review letters*, 71(22):3697, 1993.

[20] Andrew M Essin and Victor Gurarie. Bulk-boundary correspondence of topological insulators from their respective green's functions. *Physical Review B*, 84(12):125132, 2011.

[21] Mário G Silveirinha. Bulk-edge correspondence for topological photonic continua. *Physical Review B*, 94(20):205105, 2016.

[22] Guillaume Bal. Topological protection of perturbed edge states. *Communications in Mathematical Sciences*, 17(1):193–225, 2019.

[23] Guillaume Bal and Zhongjian Wang. $\mathbb{Z}_2$ classification of FTR symmetric differential operators and obstruction to Anderson localization. *Journal of Physics A: Mathematical and Theoretical*, 57(28):285202, 2024.

[24] Hermann Schulz-Baldes, Johannes Kellendonk, and Thomas Richter. Simultaneous quantization of edge and bulk Hall conductivity. *Journal of Physics A: Mathematical and General*, 33(2):L27, 2000.

[25] P Elbau and GM Graf. Equality of bulk and edge hall conductance revisited. *Communications in Mathematical Physics*, 229(3):415–432, 2002.

[26] Alexis Drouot. Microlocal analysis of the bulk-edge correspondence. *Communications in Mathematical Physics*, 383:2069–2112, 2021.

[27] Guillaume Bal. Topological charge conservation for continuous insulators. *Journal of Mathematical Physics*, 64(3):031508, 2023.

[28] Clément Tauber, Pierre Delplace, and Antoine Venaille. A bulk-interface correspondence for equatorial waves. *Journal of Fluid Mechanics*, 868:R2, 2019.

[29] Gian Michele Graf, Hansueli Jud, and Clément Tauber. Topology in shallow-water waves: a violation of bulk-edge correspondence. *Communications in Mathematical Physics*, 383:731–761, 2021.

[30] Guillaume Bal and Jiming Yu. Topological equatorial waves and violation (or not) of the bulk edge correspondence. *Journal of Physics A: Mathematical and Theoretical*, 57(40):405204, 2024.

[31] George W Hanson, S Gangaraj, and Andrei Nemilentsau. Notes on photonic topological insulators and scattering-protected edge states-a brief introduction. *arXiv preprint arXiv:1602.02425*, 2016.

[32] Samaneh Pakniyat, S Ali Hassani Gangaraj, and George W Hanson. Chern invariants of topological continua: A self-consistent nonlocal hydrodynamic model. *Physical Review B*, 105(3):035310, 2022.

[33] Hong Qin and Yichen Fu. Topological Langmuir-cyclotron wave. *Science Advances*, 9(13):8041, 2023.

[34] João C Serra and Mário G Silveirinha. Influence of spatial dispersion in the topological edge states of magnetized plasmas. *Reviews in Physics*, page 100108, 2025.

[35] Jeffrey B Parker, JW Burby, JB Marston, and Steven M Tobias. Nontrivial topology in the continuous spectrum of a magnetized plasma. *Physical Review Research*, 2(3):033425, 2020.

[36] Gian Michele Graf and Alessandro Tarantola. Boundary conditions and violations of bulk-edge correspondence in a hydrodynamic model. *arXiv preprint arXiv:2410.13940*, 2024.

[37] Gerald Teschl. *Mathematical methods in quantum mechanics*, volume 157. American Mathematical Soc., 2014.

[38] Jeffrey B Parker. Topological phase in plasma physics. *Journal of Plasma Physics*, 87(2):835870202, 2021.

[39] Thomas H Stix. *Waves in plasmas*. Springer Science & Business Media, 1992.

[40] M Marciani and P Delplace. Chiral Maxwell waves in continuous media from Berry monopoles. *Physical Review A*, 101(2):023827, 2020.

[41] S Ali Hassani Gangaraj and Francesco Monticone. Coupled topological surface modes in gyrotropic structures: Green's function analysis. *IEEE Antennas and Wireless Propagation Letters*, 17(11):1993–1997, 2018.

[42] S Ali Hassani Gangaraj and Francesco Monticone. Physical violations of the bulk-edge correspondence in topological electromagnetics. *Physical review letters*, 124(15):153901, 2020.

[43] Siddharth Buddhiraju, Yu Shi, Alex Song, Casey Wojcik, Momchil Minkov, Ian AD Williamson, Avik Dutt, and Shanhui Fan. Absence of unidirectionally propagating surface plasmon-polaritons at nonreciprocal metal-dielectric interfaces. *Nature communications*, 11(1):674, 2020.

[44] S Ali Hassani Gangaraj and Francesco Monticone. Do truly unidirectional surface plasmon-polaritons exist? *Optica*, 6(9):1158–1165, 2019.

[45] Ning Han, Jianlong Liu, Yang Gao, Keya Zhou, and Shutian Liu. Anomalous bulk-edge correspondence and dual-band topologically protected edge states in magnetized plasma. *Physical Review B*, 105(23):235411, 2022.